Experimental Neurology 317 (2019) 226–243

Contents lists available at ScienceDirect

Experimental Neurology

journal homepage: www.elsevier.com/locate/yexnr

Research paper

Upregulation of interleukin-6 on $Ca_v3.2$ T-type calcium channels in dorsal root ganglion neurons contributes to neuropathic pain in rats with spinal nerve ligation

Qingying Liu[a,c,d,1], Wen Chen[b,1], Xiaocen Fan[a], Jiaxin Wang[a], Su Fu[a], Shuang Cui[a], Feifei Liao[a], Jie Cai[a], Xinhong Wang[a], Yanhua Huang[a], Li Su[f], Lijun Zhong[f], Ming Yi[a], Fengyu Liu[a,d,*], You Wan[a,d,e,**]

[a] Neuroscience Research Institute, Peking University, Beijing 100083, China
[b] Department of Neurobiology, School of Basic Medical Sciences, Advanced Innovation Center for Human Brain Protection, Capital Medical University, Beijing 100069, China
[c] Department of Pain Management, The First Affiliated Hospital of Zhengzhou University, Zhengzhou 450052, Henan, China
[d] Department of Neurobiology, School of Basic Medical Sciences, Peking University, Beijing 100083, China
[e] Key Laboratory for Neuroscience, Ministry of Education/National Health Commission, Peking University, Beijing 100083, China
[f] Center of Medical and Health Analysis, Peking University, Beijing 100083, China

ARTICLE INFO

Keywords:
Neuropathic pain
$Ca_v3.2$ T-type calcium channel
Interleukin-6
Dorsal root ganglion
Spinal nerve ligation

ABSTRACT

The T-type calcium channels $Ca_v3.2$, one of the low voltage-activated (LVA) calcium channels, have been found to play important roles in the neuronal excitability. Recently, we and others have demonstrated that accumulation of $Ca_v3.2$ channels in the dorsal root ganglion (DRG) neurons and sensory nerves contributes to neuropathic pain after peripheral nerve injury. In the present study, we aimed to further investigate the regulation of $Ca_v3.2$ channels by interleukin-6 (IL-6) in DRG neurons in neuropathic pain rats after spinal nerve ligation (SNL). The results showed that $Ca_v3.2$ channel protein expression in L5 DRG neurons was upregulated and blockade of this channel decreased the hyperexcitability of DRG neurons and mechanical allodynia in SNL neuropathic pain rats. Furthermore, inhibition of IL-6 trans-signaling reduced the upregulation of $Ca_v3.2$ T-type channel induced by FIL-6 (a fusion protein of IL-6 and sIL-6R) in primary cultured DRG neurons *in vitro*. *In vivo*, inhibition of IL-6 trans-signaling reversed the upregulation of $Ca_v3.2$, reduced the hyperexcitability of L5 DRG neurons and alleviated mechanical allodynia in SNL rats. Our results suggest that IL-6 upregulates $Ca_v3.2$ T-type channels expression and function through the IL-6/sIL-6R trans-signaling pathway in DRG neurons, thus contributes to the development of neuropathic pain in SNL rats.

1. Introduction

It is well known that the increased excitability of the primary sensory dorsal root ganglion (DRG) neurons is a key factor in the development of peripheral neuropathic pain. T-type calcium channels, also referred to as low-voltage activated (LVA) calcium channels include three types, *i.e.*, $Ca_v3.1$, $Ca_v3.2$ and $Ca_v3.3$. The T-type channels can be opened at tiny depolarization near-resting membrane potentials

Abbreviations: AP, action potential; ANOVA, analysis of variance; AUC, area under the curve; BSA, bovine serum albumin; Cm, capacitance; CNTF, ciliary neurotrophic factor; CT, current threshold; DMEM, Dulbecco's modified Eagle medium; DMSO, dimethyl sulfoxide; DRG, dorsal root ganglion; DTT, dithiothreitol; FBS, fetal bovine serum; FIL-6, a fused IL-6/sIL-6R complex; GFAP, glial fibrillary acidic protein; gp130, glycoprotein 130; HVA, high voltage-activated; IL-6, Interleukin-6; JAK, Janus kinase; LIF, leukemia inhibitory factor; LVA, low-voltage activated; MIB, mibefradil; mIL-6R, membrane-bound IL-6R; NeuN, neuronal specific nuclear protein; NS, normal saline; OSM, oncostatin M; PB, phosphate buffer; PBS, phosphate buffered saline; PFA, paraformaldehyde; PWT, paw withdrawal threshold; Rs, series resistance; RUX, ruxolitinib; sIL-6R, soluble form of IL-6R; SDS, sodium dodecyl sulfate; SNI, spared nerve injury; SNL, spinal nerve ligation; TBST, Tris-buffered saline and Tween; TfR, transferrin receptor; TP, threshold of AP

* Correspondence to: Dr. Fengyu Liu, Neuroscience Research Institute, Peking University, 38 Xueyuan Road, Beijing 100083, China.
** Correspondence to: Dr. You Wan, Department of Neurobiology, School of Basic Medical Sciences, Peking University, Beijing 100083, China.
E-mail addresses: liufyu@bjmu.edu.cn (F. Liu), ywan@hsc.pku.edu.cn (Y. Wan).
[1] These authors contributed equally to this work.

https://doi.org/10.1016/j.expneurol.2019.03.005
Received 16 December 2018; Received in revised form 22 February 2019; Accepted 9 March 2019
Available online 11 March 2019
0014-4886/

to facilitate the generation of action potentials, and thus regulate the neuronal excitability. $Ca_v3.2$ channel is a predominant subtype in DRG neurons (Bernal Sierra et al., 2017; Bourinet et al., 2005; Talley et al., 1999), and an important regulator in nociceptive transmission (Catterall, 2010; Joksimovic et al., 2018). Evidence including ours (Kang et al., 2018) suggest that T-type calcium channels in DRG neurons contribute to neuropathic pain (Jagodic et al., 2008; Takahashi et al., 2010; Wen et al., 2010).

However, molecular mechanisms underlying the regulation of $Ca_v3.2$ T-type calcium channels in DRG neurons in chronic neuropathic pain are largely unknown.

In recent years, immune and inflammatory cytokines attract great interest in the mediation of neuropathic pain after peripheral nerve injury. Interleukin-6 (IL-6) is a pleiotropic cytokine originally identified as a B-cell stimulatory factor 2 (Hirano et al., 1985). IL-6, as well as other cytokines in its family such as IL-11, leukemia inhibitory factor (LIF), cardiotrophin-1, ciliary neurotrophic factor (CNTF), oncostatin M (OSM) and cardiotrophin-like cytokine, is characterized by exerting its biological effects *via* a common signal transduction receptor glycoprotein 130 (gp130) (Heinrich et al., 2003; Wolf et al., 2014). IL-6 performs its cellular functions through two distinct pathways: classical signaling and trans-signaling (Scheller and Rose-John, 2006). In the classical signaling pathway, IL-6 binds to the membrane-bound IL-6R (mIL-6R) to activate the family common receptor gp130 and subsequent down-stream signaling pathway (Taga and Kishimoto, 1997). The mIL-6R is expressed only on limited cell types such as hepatocytes and some leukocytes (Rose-John et al., 2006), which restricts the role of IL-6. The alternative IL-6 pathway is trans-signaling pathway in which IL-6 binds to a soluble form of IL-6R (sIL-6R) and the IL-6/sIL-6R complex stimulates a response on cells that express gp130 (Rose-John and Heinrich, 1994).

IL-6 is not only an important immunological activating factor, but also a major neuroregulin. After nerve injury, IL-6 was released in DRG and spinal dorsal horn (Latrémolière et al., 2008; Murphy et al., 1995). In the visceral inflammation process, IL-6 increased the calcium signals in the myenteric neurons (Buckley et al., 2014). In the prostate cancer cell line, IL-6 potentially regulated T-type calcium channel expression (Weaver et al., 2015).

In the present study, we aim to investigate whether IL-6 could upregulate $Ca_v3.2$ T-type channels in DRG neurons in neuropathic pain rats after peripheral nerve injury. After confirmation of the role of $Ca_v3.2$ channels in rat DRG neurons in neuropathic pain, we provide evidence that IL-6 upregulates the expression and function of $Ca_v3.2$ T-type calcium channels through the IL-6/sIL-6R trans-signaling pathway.

2. Materials and methods

2.1. Animals

Adult male Sprague Dawley rats weighing 180–220 g were purchased from the Department of Experimental Animal Sciences, Peking University Health Science Center (Beijing, China). Four animals were raised in plastic cages with corncob bedding and housed under a standard 12 h reversed light/dark cycle at 22.0 ± 1.0 °C with food and water available *ad libitum*. All animal experimental protocols were in compliance with the NIH Guide on Care and Use of Animals and followed the Guidelines of the International Association for the Study of Pain (Zimmermann, 1983). The experimental procedures were approved by the Institutional Animal Care and Use Committee of Peking University Health Science Center (LA2017116). All behavioral testing was performed in a blind manner.

2.2. Drug preparation

Two antagonists of T-type calcium channels, mibefradil (M5441, Sigma-Aldrich) and TTA-P2 (T-155, Alomone Labs), were used. Mibefradil was dissolved in normal saline (NS) to 30 mM as stock solution, and TTA-P2 was dissolved in dimethyl sulfoxide (DMSO) to 300 mM as a stock solution and the final concentration of DMSO was 1.7%. As stock solution, IL-6 (506-RL-050, R&D Systems), sIL-6R (1830-SR-025, R&D Systems) and sgp130 (an IL-6/sIL-6R signaling inhibitor, 228-GP-050, R&D Systems) were dissolved at 100 mg/ml in sterile 0.01 M phosphate buffered saline (PBS) and stored at −80 °C. Ruxolitinib [a Janus kinase (JAK) inhibitor, S1378, Selleck Chemicals] was dissolved in DMSO to 10 mM as a stock solution and the final concentration of DMSO was 0.01%.

2.3. Spinal nerve ligation (SNL) for the establishment of neuropathic pain model

The surgical procedure for L5 SNL was performed as previously described (Kim and Chung, 1992) and in our previous reports (Liu et al., 2010, 2011, 2012). Rats were randomly assigned to receive SNL or Sham operation. Briefly, rats were anesthetized with 1% pentobarbital sodium (50 mg/kg, *i.p.*), the hair of the lower back was shaved, 2 cm-long skin incision was made on the back at the left side of the L4 – S2 spine level. After removing the transverse process of the left paraspinal muscles and L5 vertebra, both L4 and L5 spinal nerves were exposed. The L5 spinal nerve was carefully isolated and tightly ligated with 6–0 silk thread 5–10 mm distal to the L5 DRG. The wound was coated with penicillin used for infection prophylaxis, and muscle and skin were sutured in two distinct layers with 3–0 silk thread. In Sham-operated rats, animals received the same operation except L5 spinal nerve ligation. In each group, the procedure by ligating the L5 spinal nerve would be taken special care to avoid any possible damage to the L4 spinal nerve or surrounding area. Aseptic surgical procedures were used to minimize unnecessary infection.

2.4. Implantation of intrathecal catheter and injection of drugs

Rats were anesthetized with 1% pentobarbital sodium (50 mg/kg, *i.p.*). Intrathecal cannula implantation was carried out as described in our previous report (Xiao et al., 2015). A guide cannula was used to puncture the dura at the cauda equina level, and a PE-10 catheter was then implanted to the lumbar enlargement level (3.5–4.0 cm rostral than the cannula) at the subarachnoid space through the cannula. The outer part of the PE-10 catheter was plugged and fixed onto the skin between the rat ears. Rats showing neurological deficits after the catheter implantation were excluded. In order to minimize the surgical injury, spinal nerve ligation and intrathecal catheter implantation were performed at the same time.

To examine effects of sgp130 (an IL-6/sIL-6R signaling inhibitor) on SNL rats, the drug sgp130 (50 ng/10 μl) was injected intrathecally to SNL rats through the implanted catheter in a 15 μl volume of solution followed by 10 μl of solution for flushing. Each injection lasted for at least 5 min. After an injection, the needle remained in site for 2 min before being withdrawn. Frequency of drug delivery is once per day from day 1 to day 3 after SNL operation. An equal volume of PBS was administrated as a control. The ipsilateral mechanical allodynia, $Ca_v3.2$ protein expression and neuron excitability were measured on day 4 after SNL.

2.5. Assessment of mechanical allodynia

Animals were acclimated to the experimental environment for 30 min every day for at least 3 days before testing. The 50% paw withdrawal threshold (PWT) in response to a series of *von* Frey hairs (North Coast Medical, Inc., Gilroy, CA) was examined by the “up and down” method (Chaplan et al., 1994) and as described previously in our lab (Chen et al., 2018). Briefly, the rats were placed individually in an inverted clear acrylic cage (18 × 8 × 8 cm), which was placed on a wire mesh and habituated for 30 min to allow acclimatization. Eight *von*

Frey hairs were chosen (0.4, 0.6, 1.0, 2.0, 4.0, 6.0, 8.0, and 15.0 g). Each trial started with a *von Frey* force of 2.0 g delivered perpendicularly to the plantar surface of the left hind-paw. An abrupt withdrawal of the foot during stimulation or immediately after the removal of the filament was recorded as a positive response. Once a positive or negative response was evoked, the next weaker or stronger filament was applied. This procedure was repeated until 6 stimuli after the first change in response had been observed. The 50% PWT was calculated using the following formula: 50% PWT = $10^{(X+kd)}/10^4$, where X is the value of the final *von Frey* filament used (in log units), k is a value measured from the pattern of positive/negative responses, and d is the average increment (in log units) between the *von* Frey hairs (Dixon, 1980). If a rat responded to the lowest *von* Frey hair, a value of 0.25 g was assigned; if a rat did not respond to the highest *von* Frey hair, the value was recorded as 15.0 g. Only those rats with 50% PWT < 4.0 g were selected and used in subsequent experiments.

2.6. Western blot analysis

2.6.1. Total protein preparation

L5 DRG tissues were homogenized and sonicated in lysis buffer containing 50 mM Tris-HCl (pH 7.4), 150 mM NaCl, 1% NP-40, 0.1% sodium dodecyl sulfate (SDS) and protease inhibitor cocktail. After being kept on ice for 1 h, the lysates were centrifuged at 12, 000 rpm for 15 min at 4 °C, then the supernatant mixing with loading buffer containing 2% SDS, 100 mM dithiothreitol (DTT), 10% glycerol and 0.25% bromophenol blue was denatured at 95 °C for 5 min and next for Western blot assay.

2.6.2. Membrane protein preparation

Membrane protein sample was prepared following the protocol (Tian et al., 2018; Tyrrell et al., 2001) as in our lab (Liu et al., 2018). Briefly, 3 or 4 L5 DRGs were homogenized in lysis buffer containing 0.3 M sucrose, 10 mM Tris pH 8.1, 2 mM EDTA, 1 mM PMSF, 1 mM DTT and protease inhibitor cocktail. After low-speed centrifugation (1000 × *g*) for 7 min at 4 °C, the homogenates were kept on ice for 1 h. Supernatant was centrifuged at high-speed centrifugation (120,000 *g*) for 1 h at 4 °C. The pellet, containing the total membrane fraction, was suspended in 0.2 M KCl and 10 mM HEPES (pH 7.4). To solubilize the membrane fraction, an equal volume of 5% Triton X-100 and 10 mM HEPES (pH 7.4) was added, and the suspension was kept on ice for 1 h. Unsolubilized material was pelleted by centrifugation at 10,000 *g* for 10 min at 4 °C, and the supernatant was collected for Western blot assay. Transferrin receptor (TfR, Life Technologies) was served as the loading control.

2.6.3. Western blot

Protein was separated on 8%–12% SDS-PAGE. The blots were blocked in 5% non-fat milk with Tris-buffered saline and Tween (TBST) (20 mM Tris-HCl, pH 7.6, 150 mM NaCl, 0.05% Tween 20), and incubated with one of the following primary antibodies at 4 °C overnight: rabbit anti-Ca_v3.2 (1: 500, H-300, Santa Cruz Biotechnology), rabbit anti-IL-6 (1: 300, ARC0062, Invitrogen), rabbit anti-IL-6R (1: 500, LS-C294926, LifeSpan Biosciences), rabbit anti-gp130 (1: 800, ab202850, Abcam), mouse anti-β-actin antibody (1: 1000, TA-09, ZSGB-Bio), rabbit anti-β-tubulin (1: 2000, 2128S, Cell signaling Technology), rabbit anti-GAPDH (1: 8000, G9545, Sigma-Aldrich), or mouse anti-TfR (1: 1000, 13–6800, Invitrogen). After washing with TBST, the membranes were incubated with one of the following secondary antibody: horseradish peroxidase-conjugated goat anti-rabbit (1: 3000, 111–035-003, Jackson ImmunoResearch) or goat anti-mouse (1: 3000, 115–035-003, Jackson ImmunoResearch) for 1 h at room temperature. Protein bands were detected using ECL reagents (Perkin Elmer) and visualized by a chemiluminescence imaging system (Tanon-5200).

2.7. Immunohistochemical analysis

2.7.1. Immunohistochemical staining

Under deep anesthesia with 1% pentobarbital sodium (50 mg/kg, *i.p.*), the rats was transcardially perfused through the aorta with 200 ml of NS at room temperature followed by 300 ml cold (4 °C) 4% paraformaldehyde (PFA) in 0.1 M phosphate buffer (PB), pH 7.4. Ipsilateral L5 DRG was rapidly dissected and postfixed in 4% PFA for 4–6 h, then cryoprotected by incubation of PB with 20% and 30% sucrose solutions at 4 °C in turn. The DRG tissue was then embedded in O.C.T. compound (Tissue-Tek), cut to 8-μm in thickness with a Leica CM 1800 cryostat and thaw-mounted onto a gelatin/chrome alum-coated glass slide. After drying in an incubator at 37 °C, the tissue sections were permeabilized in 0.01 M PBS containing 0.3% Triton X-100 for 30 min, and blocked in 10% normal goat serum with 0.3% Triton X-100 in PBS for 1 h at room temperature. The sections were then incubated with one of the following primary antibodies: rabbit anti-Ca_v3.2 antibody (1: 200, ACC-025, Alomone Labs), rabbit anti-IL-6 antibody (1: 300, ARC0062, Invitrogen), mouse anti-neuronal specific nuclear protein (NeuN, a neuronal marker, 1: 200, ab104224, Abcam) or mouse anti-glial fibrillary acidic protein (GFAP, an astrocyte marker, 1: 500, 3670S, Cell Signaling Technology) in 1% bovine serum albumin (BSA) with 0.3% Triton X-100 for 24–36 h at 4 °C. After washing with PBS 3 times, the sections were incubated with one of the following secondary antibodies: Alexa Fluor 488-conjugated goat anti-rabbit IgG (1: 500, A-11008, Invitrogen), Alexa Fluor 594-conjugated goat anti-rabbit IgG (1: 500, A-11012, Invitrogen), Alexa Fluor 568-conjugated goat anti-mouse IgG (1: 500, A-11004, Invitrogen) at room temperature for 2 h. The slide was rinsed in PBS and then dried and coverslipped with antifade mounting medium.

In our study, a polyclonal anti-Ca_v3.2 antibody (Alomone Labs, ACC-025) corresponding to residues 581–595 for immunofluorescence was used. In order to detect the specificity of the antibody, we did the antigen peptide absorption experiment of anti-Ca_v3.2. A peptide with the amino acid sequence CHVEGPQERARVAHS corresponding to residues 581–595 of the rat Ca_v3.2 protein (0.004 μg/μl) was added during the incubation step with the anti-Ca_v3.2 antibody. The staining results showed that expression of Ca_v3.2 was absent in the cells, which was similar to that of the negative control group compared with the positive group (Supplementary Fig. 1). Our results coincide with those of Becker et al. (Becker et al., 2008).

2.7.2. Immunohistochemical staining for Ca_v3.2 or gp130 on adjacent serial sections

As the antibodies of Ca_v3.2 and gp130 in our experiments were same genus source, we used slides with adjacent serial sections to observe the co-localization of these two proteins. The DRG was cut longitudinally in serial sections in 8-μm thickness. During the slicing, the first section was mounted on one glass slide coated with gelatin, and the second adjacent section was mounted on another glass slide. In this order, each two sections were pasted on two slides in series. We tried our best to keep the cell morphology similar between the two sections. After drying in an incubator at 37 °C, tissue sections were treated as the mentioned above. Briefly, after blocking, the sections were incubated with primary rabbit anti-Ca_v3.2 antibody (1: 200) and rabbit anti-gp130 antibody (1: 300, ab202850, Abcam) separately. Washing with PBS, sections were incubated with the following secondary antibodies: Alexa Fluor 488-conjugated goat anti-rabbit IgG (1: 500) and Alexa Fluor 594-conjugated goat anti-rabbit IgG (1: 500) corresponding to the primary antibody at room temperature for 2 h.

2.7.3. Confocal microscopy and image analysis

Immunofluorescent photographs were taken by a confocal laser scanning microscope (FV1000, Olympus) at 20× or 40× magnification. For quantification, 6–8 non-consecutive sections of the L5 DRG from each of 5 to 7 rats per group were imaged and counted. At least

250 labelled DRG neurons per rat were analyzed. To prevent inaccurate measurements in DRG soma cross-section, only cells with clear nuclei were counted. For the labeling methods of cell surface expression of $Ca_v3.2$ the neuron was counted as positive if more than half of its circumference was encircled by $Ca_v3.2$-immunoreactivity. The total number of $Ca_v3.2$-immunoreactivity neurons in the region of interest was counted, and the percentage of the co-localization was determined separately. DRG neurons were classified according to cross-sectional area (Liu et al., 2012; Yu et al., 2008) into three types: the small ($\leq 699\ \mu m^2$), the medium (700–1199 μm^2) and the large ($\geq 1200\ \mu m^2$). The cell area was measured using software Image-Pro Plus 6.0 (Media Cybernetics, Rockville, MD, USA) and the cell number was counted by Image J1.5 (Wayne Rasband National Institutes of Health, USA).

2.8. Primary culture of DRG neurons

Primary culture of DRG neurons was performed according to the modified method (Fang et al., 2015; Natura et al., 2005). Briefly, the rat (aged 2–3 weeks) was euthanized and its DRGs were dissected from cervical to lumbar spinal segments. The DRGs were digested with 3 mg/ml collagenase type I_A (Sigma-Aldrich) for 50 min and 0.25% trypsin (Gibco) for 15 min at 37 °C. After terminating the enzymatic treatment by Dulbecco's modified Eagle medium (DMEM) containing 10% fetal bovine serum (FBS), ganglia were dissociated with a polished Pasteur pipette and the suspension of ganglia was sieved through a filter to remove debris and centrifuged at 800 rpm for 3 min. The re-suspended cells were placed on 35-mm dishes coated with 0.5 mg/ml poly-D-lysine (Sigma-Aldrich), cultured for 3–4 h, and replaced with neurobasal growth medium containing B27 supplement, 0.5 mM L-glutamax (Sigma-Aldrich), 100 U/ml penicillin and 100 mg/ml streptomycin. The cells were cultured at 37 °C in an incubator with 5% CO_2 and 95% air. Subsequent experiments were carried out three days later. These primary cultured DRG neurons were prepared for the treatment of a fused IL-6/sIL-6R complex (FIL-6), or sgp130 for 6–12 h to investigate the effects of IL-6/sIL-6 on functional $Ca_v3.2$ T-type channels expression.

2.9. Acute dissociation of DRG neurons

DRG neurons were acutely isolated as described in our previous report (Xiao et al., 2015). Briefly, rats were deeply anesthetized and the L5 DRGs were freshly dissected. After being washed in cold DMEM, the neurons were digested with 3 mg/ml collagenase type I_A for 55 min and 0.25% trypsin for 13 min at 37 °C. The digestion was terminated with DMEM containing 10% FBS. Next, the ganglia were gently dissociated by a fire-polished Pasteur pipette and the suspension was placed on poly-D-lysine (0.5 mg/ml)-coated glass coverslips. Cells were cultured in an incubator with 95% air and 5% CO_2 at 37 °C for 3–4 h before the whole-cell patch clamp recording or the Western blot experiments.

2.10. Whole-cell patch-clamp recordings in vitro

Whole-cell patch-clamp recording was performed at room temperature using an EPC-10 amplifier with Patch-Master software (HEKA, Freiburg, Germany). Series resistance (Rs) and capacitance (Cm) values were taken directly from reading of the amplifier. Rs was compensated at least 75%. The patch pipette was pulled from borosilicate glass capillaries with a tip resistance of 4 to 9 MΩ when filled with internal solution. For the voltage-clamp recording, the external solution used to isolate Ca^{2+} currents contained (in mM): 10 $BaCl_2$, 152 TEA-Cl, and 10 HEPES adjusted pH to 7.4 with TEA-OH. To minimize contamination of T-currents with even minimal high voltage-activated (HVA) components, the HVA Ca^{2+} current was facilitated to rundown only with fluoride (F^-)-based internal solution contained (in mM): 135 TMA-OH 10 EGTA, 40 HEPES, and 2 $MgCl_2$, adjusted pH to 7.2 with hydrofluoric acid (Li et al., 2017; Nelson et al., 2007). The amplitude of T-current was measured from the peak, which was subtracted from the current at the end of the depolarizing test potential to avoid contamination with residual HVA currents that were present at more positive membrane potentials (typically at −20 mV and higher) (Messinger et al., 2009; Obradovic et al., 2014).

For the current-clamp recording, the patch pipette solution contained the following components (in mM): 110 KCl, 10 NaCl, 2 EGTA, 25 HEPES, 4 Mg-ATP and 0.3 Na_2-GTP, pH adjusted to 7.3 with KOH. The external solution contained (in mM) 128 NaCl, 2 KCl, 2 $CaCl_2$, 2 $MgCl_2$, 30 glucose, 25 HEPES, pH adjusted to 7.4 with NaOH (Zhang et al., 2014). Under the recording, the neuron was held at 0 pA, and the firing threshold of the neuron was first measured by a series of 100 ms depolarizing current injection in 5 pA steps from 0 pA to elicit the first action potential (AP). In this study, we measured current threshold (CT) and threshold of AP (TP) to evaluate intrinsic electrophysiological properties of the neuron.

To isolate T-type channel currents, the neuron was held at −70 mV and imposed voltage commands of depolarizing pulses from −110 to −40 mV in a 10-mV increment. For the activation curve, T-type channel currents were evoked by command voltage steps from the holding potential of −110 mV for 40 ms to test potentials from −80 to −20 mV for 300 ms in a 10-mV increment. For the inactivation curve, currents were evoked by a test potential to −40 mV for 300 ms after a 1-s pre-pulse at potentials ranging from −110 to −30 mV with a 10-mV increment.

The voltage dependencies of activation and steady-state inactivation were described with single Boltzmann distributions of the following formulas:

$$\text{Activation: } G(V) = G_{max}/(1 + \exp.[-(V - V_{50})/k]);$$

$$\text{Inactivation: } I(V) = I_{max}/(1 + \exp.[(V - V_{50})/k]).$$

In these formulas, G_{max} is the maximal conductance, I_{max} is the maximal amplitude of the current, V_{50} is the voltage at which half the current is activated or inactivated, and k represents the voltage dependence (slop) of the distribution. The data were analyzed using Origin 8.5 (Microcal Software, Northampton, MA).

2.11. Extracellular electrophysiological recording of ectopic discharges in vivo

Extracellular electrophysiological recording was performed as in our previous reports (Chen et al., 2018; Jiang et al., 2008; Sun et al., 2005). Briefly, rats with ligation of the L5 spinal nerve and rats with Sham-operation were anesthetized with urethane (1.5 g/kg, *i.p.*). A tracheotomy was performed and rectal temperature was kept constant at 37–38 °C. L5 dorsal root was exposed in a lower lumbar laminectomy and covered with warmed paraffin oil (37 °C) in a pool formed by skin flaps. A well around the DRG for application of mibefradil or TTA-P2 (20 μl), antagonists of T-type calcium channels, was made by agarose. The teased fiber recording method was used to record the ectopic afferent discharges entering the spinal cord along the dorsal root. Most of the dorsal muscles supplied by the dorsal ramus of the L5 spinal nerve were removed during the laminectomy.

Fine axon bundles (microfilaments) were teased from the dorsal root using specially honed No. 5 jewelers forceps (Fine Science Tools, *Inc.*, USA). Microfilaments, cut centrally but in continuity with the DRG distally, were separated from the dorsal root near its point of entry into the spinal cord, 25–30 mm central to the DRG. The cut end of the microfilament was placed on a platinum recording electrode referenced to a nearby indifferent electrode. Each microfilament was observed passively for ≥10 min for baseline testing and ≥ 60 min for topical application of antagonist-testing. Data were captured and analyzed with the Micro140 MK II and Spike 2 software (Cambridge Electronic Design, UK).

2.12. Statistical analysis

All data were presented as mean ± SEM. GraphPad Prism 5 was used for data analysis. A 2-tailed unpaired *t*-test was used for the comparison of the mean between two groups. One-way analysis of variance (ANOVA) or two-way ANOVA followed by Bonferroni *post hoc* test was used for multiple comparisons. Differences with $p < 0.05$ were considered statistically significant.

3. Results

3.1. Increased total and membrane $Ca_v3.2$ protein expression in L5 DRG neurons after SNL

We first established the rat model of neuropathic pain with L5 SNL operation. Rats after ligation of the left L5 spinal nerve developed mechanical allodynia in the ipsilateral hind paw within 1 day and lasted 21 days [group effect: $F_{(1,\ 90)} = 77.10$, $p < 0.001$; time effect: $F_{(5,\ 90)} = 28.09$, $p < 0.001$; interaction: $F_{(5,\ 90)} = 19.90$, $p < 0.001$, Supplementary Fig. 2], as similar to our previous reports (Liu et al., 2012, 2018).

To explore the expression changes of $Ca_v3.2$ in neuropathic pain rats, we examined $Ca_v3.2$ protein expression with Western blotting in L5 DRGs at 1, 3, 7, 14 and 21 days after SNL. As shown in Fig. 1A, $Ca_v3.2$ total protein expression increased significantly from day 1 to day 21 in the SNL rats compared with that in the Sham-operated rats [group effect: $F_{(1,\ 48)} = 71.17$, $p < 0.001$; time effect: $F_{(4,\ 48)} = 2.90$, $p < 0.05$; interaction: $F_{(4,48)} = 0.46$, $p > 0.05$, two-way ANOVA followed by Bonferroni's *post hoc* test]. In addition, we examined the membrane expression of $Ca_v3.2$ proteins at day 3 after nerve injury. It was found that the membrane $Ca_v3.2$ also increased significantly at day 3 after L5 SNL [$t_{(12)} = 4.31$, $p < 0.01$, unpaired *t*-test, Fig. 1B].

In order to visualize the $Ca_v3.2$ membrane expression, we used immunohistochemical staining to further examine the cellular localization of $Ca_v3.2$ in DRG neurons. Our results indicated that $Ca_v3.2$ was expressed in the membrane of all three categories of DRG neurons after SNL (Fig. 1C), the percentage of neurons with $Ca_v3.2$ membrane expression increased significantly at days 1, 3 and 14 after SNL [group effect: $F_{(1,\ 16)} = 45.62$, $p < 0.001$; time effect: $F_{(2,\ 16)} = 0.13$, $p > 0.05$; interaction: $F_{(2,\ 16)} = 0.68$, $p > 0.05$, two-way ANOVA followed by Bonferroni's *post hoc* test, Fig. 1D] than that after Sham-operation.

We next examined the expression patterns of membrane $Ca_v3.2$ in the DRG neurons. For quantification analysis, the ratio of membrane $Ca_v3.2$-positive neurons significantly increased at days 1, 3 and 14 after SNL within small [$F_{(3,\ 26)} = 7.40$, $p < 0.001$, one-way ANOVA followed by Bonferroni's *post hoc* test], the medium-sized [$F_{(3,\ 26)} = 13.77$, $p < 0.001$, one-way ANOVA followed by Bonferroni's *post hoc* test] and large [$F_{(3,\ 26)} = 21.75$, $p < 0.001$, one-way ANOVA followed by Bonferroni's *post hoc* test] neurons compared with that after Sham-operation (Fig. 1E). Area frequency histograms also showed that membrane $Ca_v3.2$-positive neurons increased significantly after SNL (Fig. 1F). These results demonstrate that $Ca_v3.2$ channel expression is upregulated in L5 DRG neurons in neuropathic pain rats after SNL. As shown in Fig. 1A and Supplementary Fig. 2, L5 SNL operation caused a stable pain behavior and increased $Ca_v3.2$ protein expression from day 3 to day 21 after nerve injury. Accordingly, the day 3 after nerve injury was chosen as the representative time point in the following electrophysiological and behavioral experiments.

3.2. Increased T-type calcium channel currents in L5 DRG neurons after SNL

$Ca_v3.2$ distributed mainly in the cytoplasm of DRG neurons in Sham-operation rats, while turned to the membrane of the damaged DRG neurons in SNL rats (Fig. 1C). It is well known that ion channels in the membrane are functional compared to those in the cytoplasm in a neuron, so we examined T-type calcium channel currents in DRG neurons.

Our results (Fig. 1) demonstrated that small-, the medium-sized and large DRG neurons expressed $Ca_v3.2$ in Sham-operation and SNL rats. In the following experiment, small DRG neurons (< 30 μm in diameter) were chosen as the representative in patch clamp recording. Consistent with the increase of $Ca_v3.2$ membrane protein, the density of T-type calcium currents was also significantly increased in L5 DRG neurons 3 days after SNL compared with that after Sham-operation [$t_{(41)} = 2.78$, $p < 0.01$, unpaired *t*-test, Fig. 2A and B].

It is well known that the voltage-dependent or steady-state activation and inactivation are important electrophysiological properties of T-type Ca^{2+} channels and influence the neuronal excitability (Jagodic et al., 2007). Thus, we examined the changes of activation and inactivation of T-type channels in DRG neurons in neuropathic pain rats after SNL. It was found that the activation curve was hyperpolarized, *i.e.*, the V_{50} left-shifted from −30.48 ± 1.98 mV in the Sham-operation group to −40.87 ± 1.12 mV in the SNL group [$t_{(21)} = 4.94$, $p < 0.001$, unpaired *t*-test, Fig. 2C], whereas inactivation properties showed no obvious changes [−71.25 ± 1.97 mV *vs.* -67.21 ± 1.69 mV, SNL group *vs.* Sham-operation group, $t_{(16)} = 1.56$, $p > 0.05$, unpaired *t*-test, Fig. 2D]. These results indicate that the hyperpolarizing shift of the voltage dependence of activation may account for the increase in T-type currents in DRG neurons in SNL-induced neuropathic pain rats.

3.3. Inhibition T-type calcium channel suppresses the ectopic discharges in the injured DRG neurons of SNL rats

Next, using extracellular electrophysiological recording technique, we evaluated the effects of two T-type calcium channel antagonists (mibefradil and a more preferential blocker, TTA-P2) on the ectopic discharges in the injured DRG neurons at days 3 after SNL. As shown in Fig. 3, mibefradil applying to DRG neurons (3 mM, 5 mM, 10 mM) produced a dose-dependent decrease of the frequency of ectopic discharges in SNL rats [group effect: $F_{(3,\ 2730)} = 4.66$, $p < 0.01$; time effect: $F_{(35,\ 2730)} = 26.12$, $p < 0.001$; interaction: $F_{(105,2730)} = 3.40$, $p < 0.001$, two-way ANOVA followed by Bonferroni's *post hoc* test, Fig. 3A, C–D]. As shown by analysis with area under the curve (AUC) values (0 to 60 min of the analysis time), mibefradil at 10 mM had significantly inhibitory effects than NS in SNL rats [$F_{(3,\ 78)} = 4.63$, $p < 0.01$, one-way ANOVA followed by Bonferroni's *post hoc* test, Fig. 3B]. Mibefradil at 10 mM had no obvious effects on the discharge frequency and AUC values in Sham-operated rats (Fig. 3E–H).

To confirm the mibefradil results, we further tested the effect of TTA-P2, another more specific blocker of T-type calcium channels, on ectopic discharges in the DRG neurons. Similarly, in SNL rats, TTA-P2 (0.5 mM, 1.5 mM, 5 mM) also dose-dependently inhibited the frequency of ectopic discharges when compared with DMSO treatment control. TTA-P2 at 5 mM significantly inhibited the frequency of ectopic discharges [group effect: $F_{(3,\ 2275)} = 45.62$, $p < 0.001$; time effect: $F_{(35,\ 2275)} = 0.13$, $p < 0.001$; interaction: $F_{(105,\ 2275)} = 0.68$, $p < 0.001$, two-way ANOVA followed by Bonferroni's *post hoc* test, Fig. 4A, C–D]. Analysis with AUC values clearly exhibited the significantly inhibitory effects of TTA-P2 as compared with in DMSO treatment in SNL rats [$F_{(3,\ 65)} = 10.47$, $p < 0.001$, one-way ANOVA followed by Bonferroni's *post hoc* test, Fig. 4B]. In contrast, in Sham-operation rats, TTA-P2 at 5 mM had no obvious effects on the discharge frequency and AUC values (Fig. 4E–H). These results suggest that T-type calcium channels contribute to increase of the excitability of DRG neurons in neuropathic pain rats after SNL.

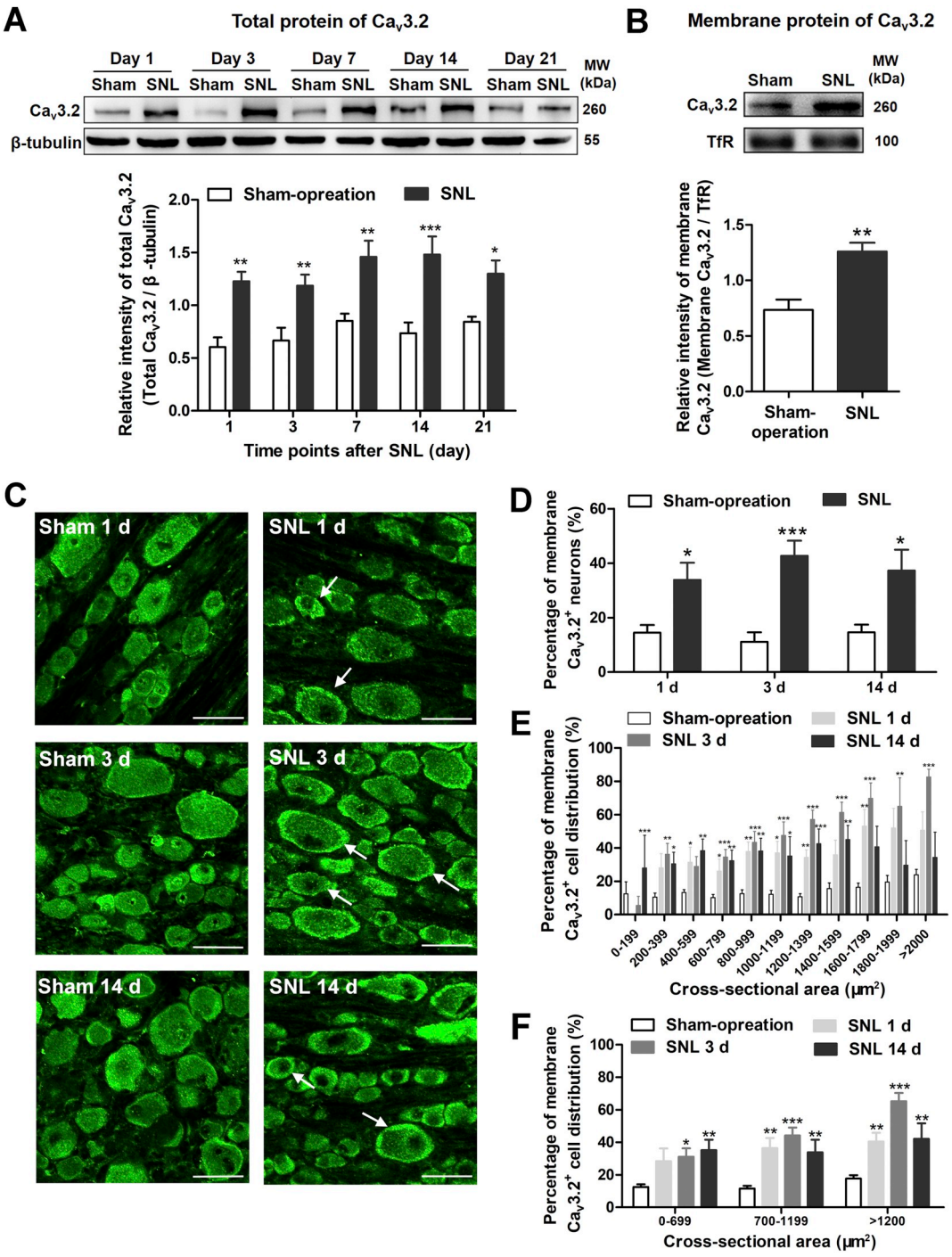

Fig. 1. Increased expression of $Ca_v3.2$ in DRG neurons in SNL rats.

(A) Total protein expression of $Ca_v3.2$. Upper: representative Western blot bands; lower: statistical analysis of total protein expression. The expression of total protein expression increased significantly in DRG neurons from day 1 to day 21 in SNL rats compared to Sham-operation rats. n = 7. *p < 0.05, ** p < 0.01, ***p < 0.001, two-way ANOVA with Bonferroni's *post hoc* test. (B) Membrane protein expression of $Ca_v3.2$ in DRG neurons in rats 3 days after SNL as an example. Upper: representative Western blot bands; lower: statistical analysis of membrane protein expression. Membrane protein increased significantly in SNL group compared with Sham-operation group. n = 7. **p < 0.01, unpaired *t*-test. (C) Immunofluorescence staining showed expression of $Ca_v3.2$ in the L5 DRG at days 1, 3, and 14 after SNL or Sham-operation. Arrows indicate membrane $Ca_v3.2$ positive neurons. Scale bar = 50 μm. (D) Quantification analysis of neurons with membrane $Ca_v3.2$ positive over total neurons. Number of neurons with membrane $Ca_v3.2$ positive increased in SNL group compared with Sham-operation group. n = 5. *p < 0.05, ***p < 0.001, two-way ANOVA with Bonferroni's *post hoc* test. (E) Percentage of membrane $Ca_v3.2$ positive neurons over total $Ca_v3.2$ positive neurons with an arbitrary 200-μm^2 subdivision of cross-sectional areas. n = 5. *p < 0.05, **p < 0.01, ***p < 0.001, one-way ANOVA followed by Bonferroni's *post hoc* test. (F) Percentage of membrane $Ca_v3.2$ positive neurons over total $Ca_v3.2$ positive neurons in small, the medium-sized, or large DRG neurons. Note that the percentage of membrane $Ca_v3.2$ positive neurons increased significantly in all types of neurons at days 1, 3, 14 after SNL compared with Sham-operation. n = 5. *p < 0.05, **p < 0.01, ***p < 0.001, one-way ANOVA followed by Bonferroni's *post hoc* test.

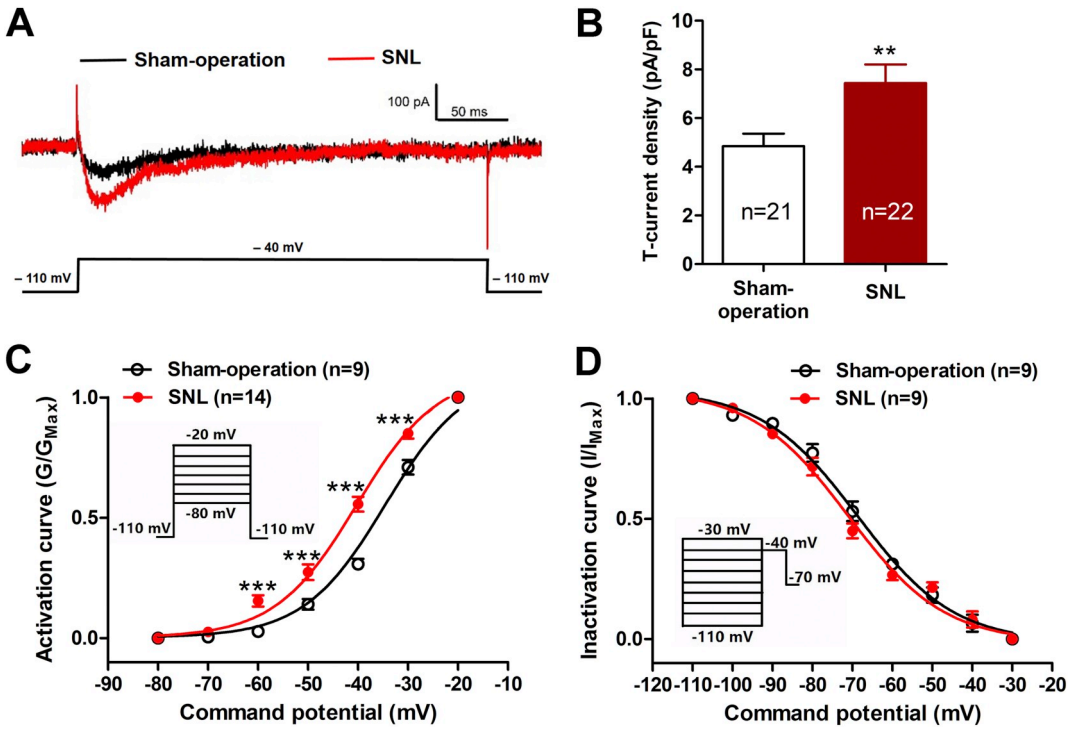

Fig. 2. Upregulation of the T-type calcium currents in acutely isolated DRG neurons in SNL rats.
(A) Representative traces of T-type calcium currents in the Sham-operation and SNL rats 3 days after surgery. (B) Statistical analysis. T-type calcium current densities (in pA/pF) increased in SNL rats compared with that in Sham-operation rats. n = 21–22, **p < 0.01, unpaired *t*-test. (C) The activation curve. A left-shifting of the steady-state activation curve indicated the increased channel availability. n = 9–14, ***p < 0.001, two-way ANOVA followed by Bonferroni's *post hoc* test. (D) The inactivation curve. No obvious differences were observed between SNL group and Sham-operation group. n = 9, two-way ANOVA followed by Bonferroni's *post hoc* test.

3.4. T-type calcium channel inhibition attenuates pain hypersensitivity in SNL neuropathic pain rats

Intrathecal administration of T-type calcium channel antagonist mibefradil attenuated the mechanical allodynia at 3 days after SNL (Fig. 5A). It was found that mibefradil at 10 mM significantly reversed 50% PWTs 1 h after the application, and this effect disappeared at 4 h in rats 3 days after SNL [group effect: $F_{(2,\ 42)} = 6.30$, $p < 0.01$; time effect: $F_{(2,\ 42)} = 18.53$, $p < 0.001$; interaction: $F_{(4,42)} = 5.54$, $p < 0.01$, two-way ANOVA followed by Bonferroni's *post hoc* test, Fig. 5A]. Furthermore, we examined the effects the mibefradil on mechanical allodynia at 14 days after SNL. Similarly, mibefradil also showed analgesic effects at 14 days after SNL [group effect: $F_{(2,\ 42)} = 1.99$, $p > 0.05$; time effect: $F_{(2,\ 42)} = 12.45$, $p < 0.001$; interaction: $F_{(4,42)} = 7.40$, $p < 0.001$, two-way ANOVA followed by Bonferroni's *post hoc* test, Fig. 5B]. These results suggest that inhibition of T-type calcium channel reduces pain hypersensitivity, and T-type channels are involved in neuropathic pain 3 days and 14 days after SNL.

3.5. Upregulation of IL-6 and gp130 in L5 DRG neurons in SNL rats

To investigate the regulatory effect of IL-6 in the membrane expression of $Ca_v3.2$ in DRG neurons of SNL neuropathic pain rats, we first examined the change of IL-6 expression in L5 DRG. As shown in Fig. 6A, the IL-6 expression increased significantly from day 1 to day 21 in SNL rats when compared with that in Sham-operation rats [group effect: $F_{(1,48)} = 112.6$, $p < 0.001$; time effect: $F_{(4,48)} = 1.59$, $p > 0.05$; interaction: $F_{(4,48)} = 2.03$, $p > 0.05$; two-way ANOVA followed by Bonferroni's *post hoc* test]. In addition, we used double immunofluorescence staining to examine the IL-6 expressing cell types in L5 DRG in SNL rats with cell-specific markers: NeuN (a marker of neuron) and GFAP (a marker of satellite glial cell). The results showed that IL-6 was distributed in both neurons and satellite glial cells 3 days after SNL (Fig. 6B).

IL-6 exerts its biological activities through two molecules, an IL-6-specific receptor (mIL-6R or sIL-6R) and a signal transducer, gp130 (Rose-John, 2012; Rothaug et al., 2016). In rat DRG, sIL-6R but not mIL-6R was detected (Fang et al., 2015). So we focused on the changes of sIL-6R and gp130 in L5 DRG neurons.

With Western blotting assay, it was shown that sIL-6R expression had no obvious changes in SNL rats compared with Sham-operation rats [group effect: $F_{(1,48)} = 1.48$, $p > 0.05$; time effect: $F_{(4,48)} = 3.38$, $p < 0.05$; interaction: $F_{(4,48)} = 0.38$, $p > 0.05$; two-way ANOVA followed by Bonferroni's *post hoc* test, Fig. 6C], but gp130 increased significantly from day 1 to day 21 in SNL rats compared with that in Sham-operation rats [group effect: $F_{(1,48)} = 110.80$, $p < 0.001$; time effect: $F_{(4,48)} = 0.59$, $p > 0.05$; interaction: $F_{(4,48)} = 0.10$, $p > 0.05$; two-way ANOVA followed by Bonferroni's *post hoc* test, Fig. 6D]. These results suggest that IL-6 exerts its effects through trans-signaling in DRG neurons of neuropathic pain rats after SNL.

3.6. Co-localization of $Ca_v3.2$ and gp130 in DRG neurons

Existence of common receptor gp130 on the membrane of $Ca_v3.2$ expressing DRG neurons is the basis for the IL-6-induced up-regulation of $Ca_v3.2$ channels. Therefore, we examined the co-localization of gp130 receptor and $Ca_v3.2$ in DRG neurons. As shown in Fig. 6E, double immunofluorescent staining showed that gp130 co-localized with $Ca_v3.2$ in DRG neurons in both Sham-operation and SNL rats. This result provides a morphological basis for the action of IL-6.

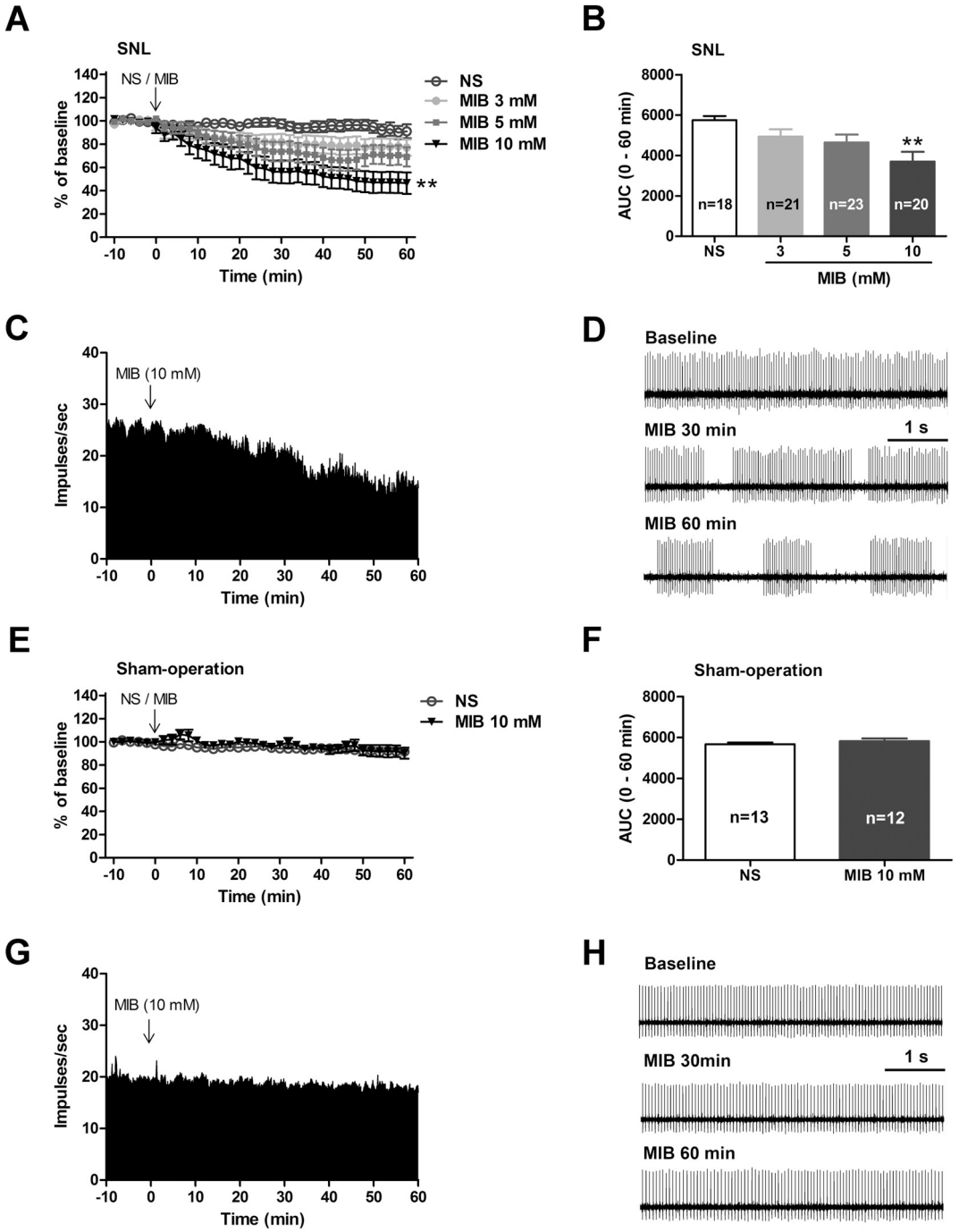

Fig. 3. Inhibition of T-type Ca^{2+} channel with mibefradil (MIB) suppressed the frequency of ectopic discharges from injured DRG neurons in SNL rats.
(A) Effects of mibefradil (3, 5, and 10 mM) on the ectopic discharges from injured DRG neurons in SNL rats. Note that 10 mM mibefradil significantly suppressed the firing frequency compared with NS group. **p < 0.01, two-way ANOVA followed by Bonferroni's *post hoc* test. (B) Statistical analysis with the area under the time-course curve (AUC) in (A). 10 mM mibefradil significantly reduced the AUC compared with NS group. n = 18–23. **p < 0.01, one-way ANOVA followed by Bonferroni's *post hoc* test. (C, D) An example of the frequency-time histogram of ectopic discharges before and after application of mibefradil at 10 mM from a single fiber in the SNL rat. (E) Effects of mibefradil (10 mM) on the spontaneous discharges from normal DRG neurons in Sham-operation rats. Note that 10 mM mibefradil had no obvious effects on discharge frequency. Two-way ANOVA followed by Bonferroni's *post hoc* test. (F) Statistical analysis with the AUC in (E). 10 mM mibefradil had no obvious effects on the AUC. n = 12–13. (G, H) An example of the frequency-time histogram of spontaneous discharges before and after application of mibefradil at 10 mM from a single fiber in the Sham-operation rat.

3.7. Activation of IL-6/sIL-6R trans-signaling with FIL-6 upregulates $Ca_v3.2$ expression in primary cultured DRG neurons

To further validate whether IL-6 mediated trans-signaling contributed to $Ca_v3.2$ membrane expression, we investigated the effect of IL-6/sIL-6R activation on $Ca_v3.2$ expression by application of FIL-6 [a mixture of IL-6 (50 ng/ml) with sIL-6R (50 ng/ml)] to primary cultured DRG neurons for 6–12 h. As shown in Fig. 7A, FIL-6 produced a significant increase in total $Ca_v3.2$ proteins from 6 to 12 h after FIL-6 application compared with that after PBS treatment [$F_{(2,\ 18)} = 12.49$, $p < 0.001$, one-way ANOVA followed by Bonferroni's *post hoc* test]. Considering the functional significance of membrane $Ca_v3.2$ channels,

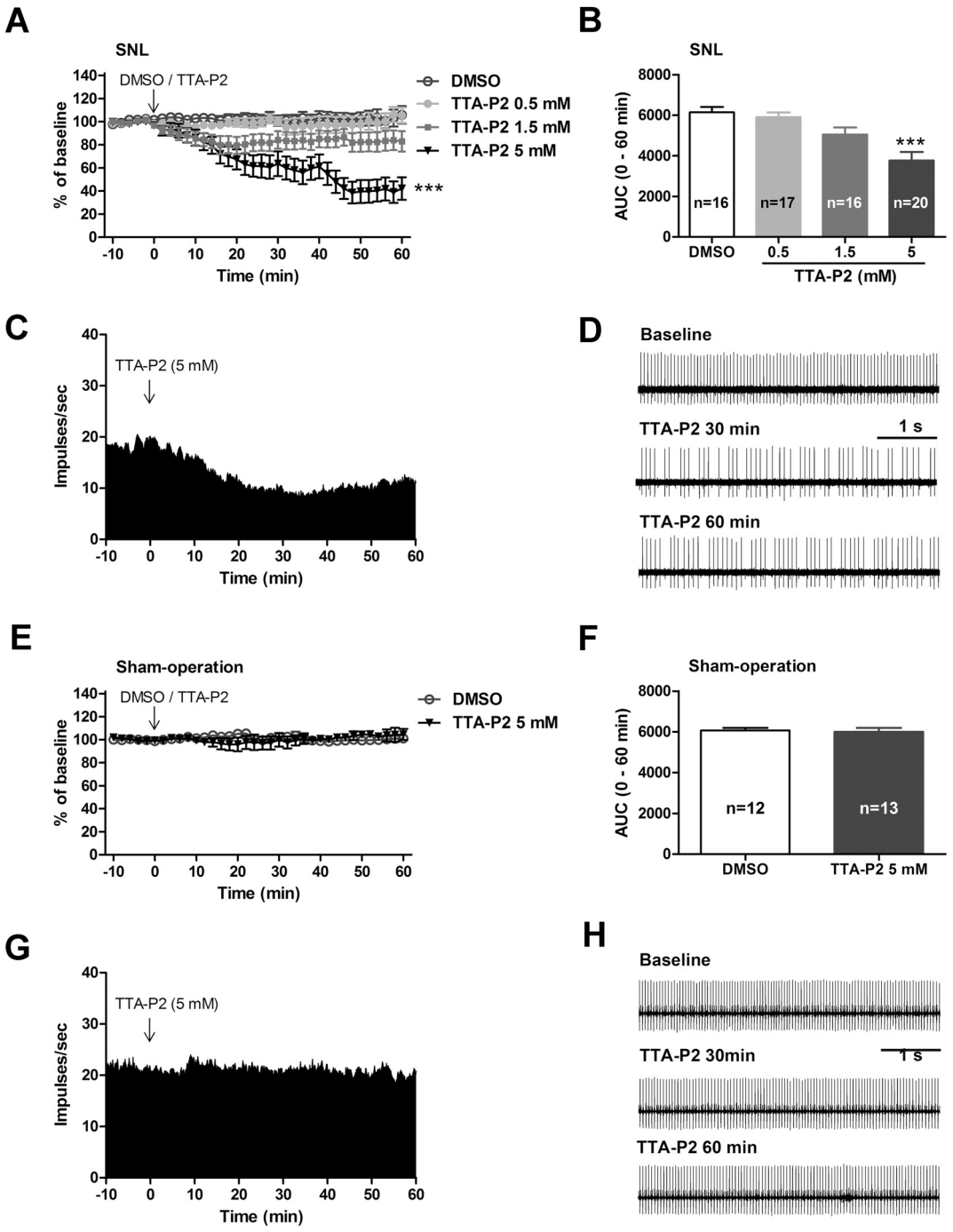

Fig. 4. Inhibition of T-type Ca^{2+} channel with TTA-P2 suppressed the frequency of ectopic discharges from injured DRG neurons in SNL rats.
(A) Effects of TTA-P2 (0.5, 1.5, and 5 mM) on the ectopic discharges from injured DRG neurons in SNL rats. Note that 5 mM TTA-P2 significantly suppressed the firing frequency compared with DMSO group. ***p < 0.001, two-way ANOVA followed by Bonferroni's *post hoc* test. (B) Statistical analysis with the AUC in (A). 5 mM TTA-P2 significantly reduced the AUC compared with DMSO group. n = 16–20. *** p < 0.001, one-way ANOVA followed by Bonferroni's *post hoc* test. (C, D) An example of the frequency-time histogram of ectopic discharges before and after application of TTA-P2 at 5 mM from a single fiber in the SNL rat. (E) Effects of TTA-P2 (5 mM) on the spontaneous discharges from normal DRG neurons in Sham-operation rats. Note that 5 mM TTA-P2 had no obvious effects on spontaneous discharge frequency. Two-way ANOVA followed by Bonferroni's *post hoc* test. (F) Statistical analysis with the AUC in (E). 5 mM TTA-P2 had no obvious effects on the AUC. n = 12–13. (G, H) An example of the frequency-time histogram of spontaneous discharges before and after application of TTA-P2 at 5 mM from a single fiber in the Sham-operation rat.

we further examined the membrane expression of $Ca_v3.2$ protein. Consistent with the changes in the total $Ca_v3.2$, FIL-6 (50 ng/ml) incubation for 6 h induced a significant increase of membrane $Ca_v3.2$ protein in the cultured DRG neurons [$F_{(2,\ 15)} = 8.85$, $p < 0.01$, one-way ANOVA followed by Bonferroni's *post hoc* test, Fig. 7B].

We next tested the effect of sgp130 on the effect of the FIL-6-induced $Ca_v3.2$ expression in cultured DRG neurons. The results showed that sgp130 (50 ng/ml) pretreatment for 10 min significantly reversed the FIL-6-induced upregulation of total (Fig. 7C) and membrane $Ca_v3.2$ expression (Fig. 7D). The total $Ca_v3.2$ expression decreased in the sgp130 + FIL-6 group as compared with the PBS + FIL-6 group [$t_{(4)} = 5.76$, $p < 0.01$, unpaired *t*-test, Fig. 7C]. Similarly,

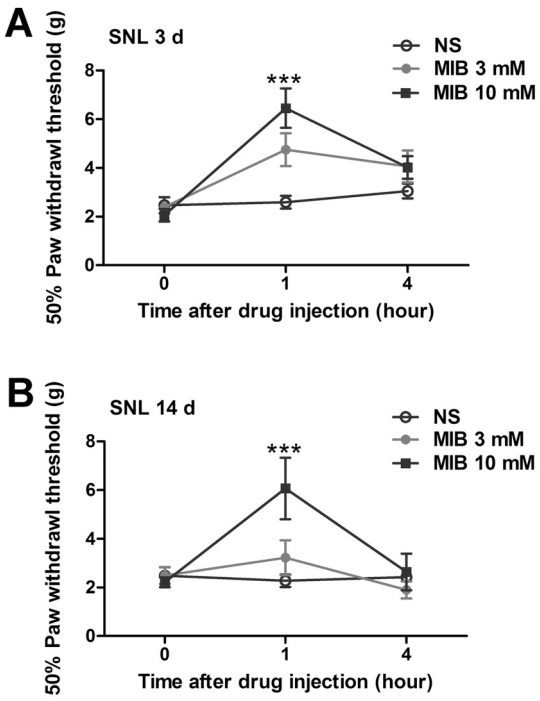

Fig. 5. Mibefradil, a T-type Ca^{2+} channel blocker, alleviated mechanical allodynia in SNL rats.
Intrathecal application of mibefradil (10 mM) significantly attenuated mechanical allodynia on 3 days (A) and 14 days (B) after SNL compared with NS group. n = 8. *** $p < 0.001$, two-way ANOVA with Bonferroni's *post hoc* test. These data indicated that the effect of mibefradil became maximal within 1 h and returned to baseline within 4 h.

$Ca_v3.2$ membrane expression was also decreased in sgp130 + FIL-6 group compared to that in PBS + FIL-6 group [$t_{(4)} = 6.12$, $p < 0.01$, unpaired *t*-test, Fig. 7D]. Representative immunofluorescent staining imagings of $Ca_v3.2$ membrane expression in FIL-6 treatment group and sgp130 + FIL-6 treatment group were shown in Fig. 7E.

Furthermore, we examined whether FIL-6 could induce a functional upregulation of $Ca_v3.2$ channels using whole-cell patch-clamp recording technique. We found that FIL-6 significantly upregulated the T-type calcium channel currents in the primary cultured DRG neurons. As shown in Fig. 8, FIL-6 incubation (50 ng/ml) for 6 h caused a significant increase in T-type Ca^{2+} current amplitude compared with the PBS control [$t_{(38)} = 3.28$, $p < 0.01$, unpaired *t*-test, Fig. 8A and B], and this FIL-6-induced upregulation of T-type calcium currents was reversed by sgp130 [$t_{(39)} = 2.89$, $p < 0.01$, unpaired *t*-test, Fig. 8A and B]. According to the activation curve, FIL-6 caused a left-shifting of the activation curve compared with the PBS [-39.09 ± 0.78 mV *vs.* -36.31 ± 0.70 mV, PBS + FIL-6 group *vs.* PBS group, $t_{(28)} = 2.65$, $p < 0.05$, unpaired *t*-test, Fig. 8C], while sgp130 had no effect on the FIL-6-induced left-shifting of activation curve (-39.94 ± 1.14 mV *vs.* -39.09 ± 0.78 mV, sgp130 + FIL-6 group *vs.* PBS + FIL-6 group, $t_{(28)} = 2.65$, $p > 0.05$, unpaired *t*-test, Fig. 8C). Additionally, by the inactivation curve of T-type calcium currents, FIL-6 had no obvious effects, and accordingly sgp130 showed no significant reversal [-68.28 ± 0.88 mV *vs.* -65.41 ± 1.74 mV, PBS + FIL-6 group *vs.* PBS group, $t_{(32)} = 1.52$, $p > 0.05$; -65.59 ± 1.91 mV *vs.* -68.28 ± 0.88 mV, sgp130 + FIL-6 group *vs.* PBS + FIL-6 group, $t_{(32)} = 1.33$, $p > 0.05$, unpaired *t*-test, Fig. 8D]. These data indicate that IL-6 *via* its trans-signaling pathway promotes the membrane expression and functional upregulation of T-type Ca^{2+} channels in the primary culture DRG neurons.

3.8. Blockade of IL-6 downstream signal pathway inhibits FIL-6-induced upregulation of $Ca_v3.2$ T-type calcium channels in primary cultured DRG neurons

We next investigated the effects of ruxolitinib, an inhibitor of JAK which is the upstream molecule of the IL-6 intracellular signaling pathway, on the expression and function of $Ca_v3.2$ T-type calcium channels *in vitro*. The results showed that ruxolitinib (1 μM) application 1 h before FIL-6 incubation significantly reversed the FIL-6 upregulation on the total [$t_{(10)} = 2.69$, $p < 0.1$, unpaired *t*-test, Fig. 9A] and membrane expression of $Ca_v3.2$ [$t_{(10)} = 5.15$, $p < 0.001$, unpaired *t*-test, Fig. 9B] in the cultured DRG neurons. Coincidently, as shown in Fig. 9C and D, ruxolitinib also reversed the FIL-6-upregulated T-type calcium current density [$t_{(24)} = 2.82$, $p < 0.01$, unpaired *t*-test].

In addition, ruxolitinib reversed the FIL-6-induced left-shifting of steady-state activation curve [-45.59 ± 0.91 mV *vs.* -42.06 ± 1.33 mV, DMSO + FIL-6 group *vs.* DMSO + PBS group, $t_{(14)} = 2.19$, $p < 0.05$; -40.00 ± 0.71 mV *vs.* -45.59 ± 0.91 mV, Rux + FIL-6 group *vs.* DMSO + FIL-6 group, $t_{(15)} = 4.88$, $p < 0.001$, unpaired *t*-test, Fig. 9E], but had no obvious effects on the inactivation curve of T-type channel currents [-67.94 ± 1.38 mV *vs.* -68.51 ± 2.14 mV, DMSO + FIL-6 group *vs.* DMSO + PBS group, $t_{(17)} = 0.22$, $p > 0.05$; -66.66 ± 2.35 mV *vs.* -67.94 ± 1.38 mV, Rux + FIL-6 group *vs.* DMSO + FIL-6 group, $t_{(18)} = 0.44$, $p > 0.05$, unpaired *t*-test, Fig. 9F].

3.9. Inhibition of IL-6/sIL-6R trans-signaling reduces upregulation of $Ca_v3.2$ T-type calcium channel expression, hyperexcitability of DRG neurons and pain hypersensitivity in SNL rats

To further validate whether or not IL-6/sIL-6 trans-signaling was involved in the development of SNL-induced neuropathic pain through membrane $Ca_v3.2$, we used sgp130 (an inhibitor of IL-6/sIL-6 trans-signaling, 50 ng/10 μl, once per day from day 1 to day 3 after operation) to probe the role of IL-6. First, we investigated the effects of sgp130 on expression of $Ca_v3.2$ in SNL rats. As shown in Fig. 10A and B, sgp130 for 3 days significantly inhibited the SNL-induced total $Ca_v3.2$ proteins [$t_{(10)} = 3.31$, $p < 0.01$, unpaired *t*-test, Fig. 10A] and membrane $Ca_v3.2$ proteins [$t_{(8)} = 3.90$, $p < 0.01$, unpaired *t*-test, Fig. 10B] in DRG neurons compared with the PBS treatment group in SNL rats.

Furthermore, sgp130 significantly inhibited the hyperexcitability of DRG neurons in SNL neuropathic pain rats. For instance, the current threshold (CT) to evoke action potentials decreased significantly in SNL DRG neurons [$t_{(34)} = 3.53$, $p < 0.001$, unpaired *t*-test], but sgp130 could reverse this effect [$t_{(37)} = 3.50$, $p < 0.001$, unpaired *t*-test, Fig. 10C and D]. Consistently, sgp130 reversed the decline of the threshold of action potential (TP) [$t_{(37)} = 4.22$, $p < 0.001$, unpaired *t*-test, Fig. 10E].

Morever, the behavioral results showed that intrathecal application of sgp130 (50 ng/10 μl) significantly attenuated the SNL-induced mechanical allodynia. After L5 SNL, 50% PWTs decreased significantly in the ipsilateral hindpaw of the SNL rats [$t_{(27)} = 35.44$, $p < 0.001$, unpaired *t*-test], and sgp130 significantly reversed this effect [$t_{(27)} = 8.61$, $p < 0.001$, unpaired *t*-test, Fig. 10F].

These above results indicate that IL-6 mediated trans-signaling contributes to the upregulation of $Ca_v3.2$ T-type calcium channels after SNL, sgp130 inhibition of IL-6/sIL-6R trans-signaling decreases the expression of $Ca_v3.2$ T-type calcium channels, then suppresses the hyperexcitability of DRG neurons and alleviates mechanical allodynia in SNL neuropathic pain rats.

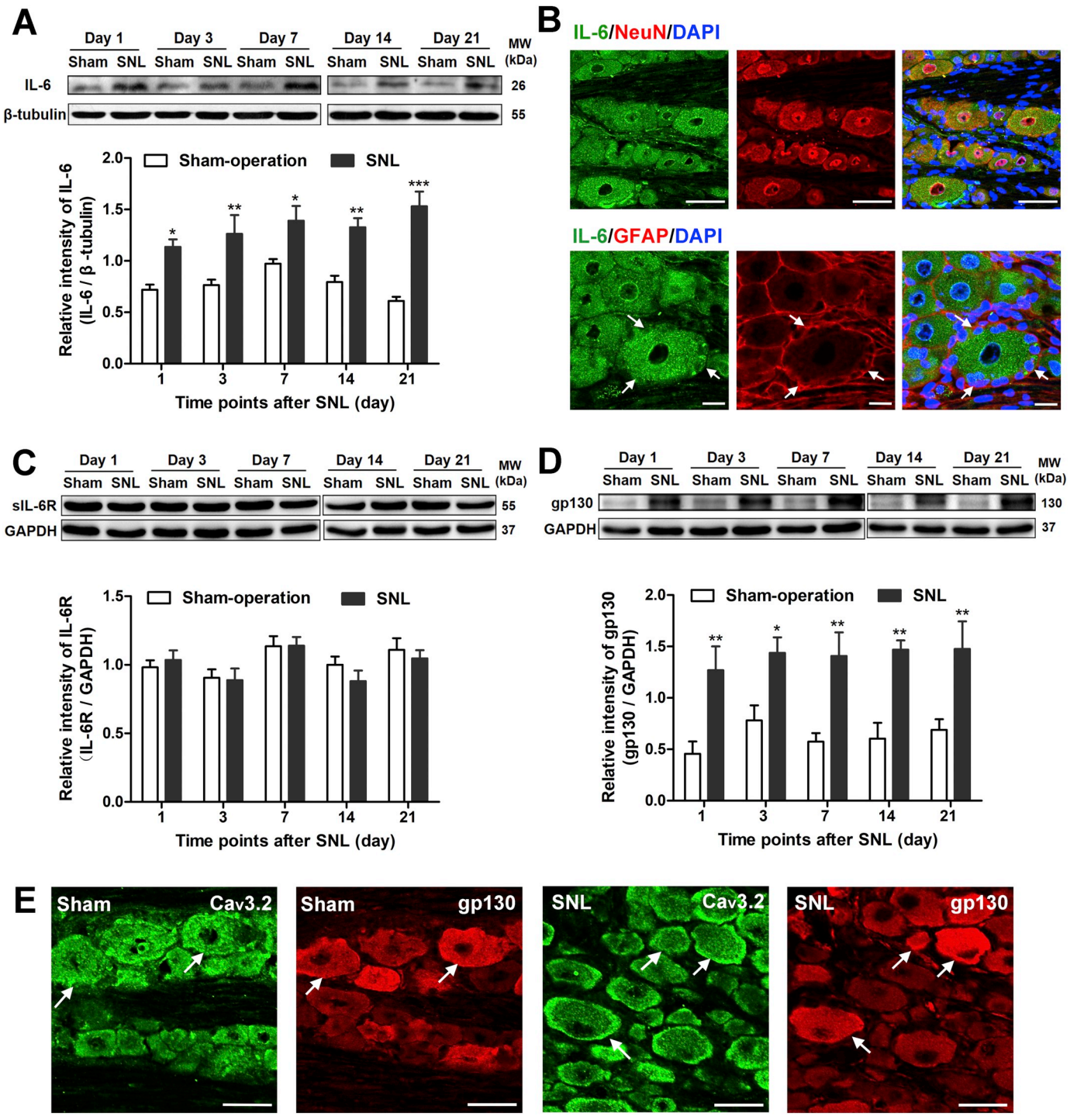

Fig. 6. Expression of IL-6, sIL-6 receptor, gp130 and $Ca_v3.2$ in DRG neurons of SNL rats.
(A) IL-6 Western blotting detection. Upper: representative Western blot bands of IL-6; lower: statistical analysis of the relative band intensities of IL-6. The expression of IL-6 increased significantly in DRG neurons from day 1 to day 21 in SNL rats compared to Sham-operation rats. n = 7. *p < 0.05, **p < 0.01, ***p < 0.001, two-way ANOVA with Bonferroni's *post hoc* test. (B) IL-6 cellular distribution in the DRG. Double immunofluorescence staining showed co-localization of IL-6 (green) with NeuN (red) and GFAP (red). Arrowheads point to co-localization of IL-6 and GFAP. Upper: scale bar = 50 μm; lower: scale bar = 20 μm. (C) sIL-6R Western blotting detection. Upper: representative Western blot bands; lower: statistical analysis of the relative intensities of sIL-6R. No significant differences were observed on the expression of sIL-6R between Sham-operation and SNL group. n = 7, two-way ANOVA with Bonferroni's *post hoc* test. (D) gp130 Western blotting detection. Upper: representative Western blot bands; lower: statistical analysis of the relative intensities of gp130. The expression of gp130 increased significantly in DRG neurons from day 1 to day 21 in SNL rats compared to Sham-operation rats. n = 7. *p < 0.05, **p < 0.01, two-way ANOVA with Bonferroni's *post hoc* test. (E) Representative immunofluorescence images showing the co-localization of $Ca_v3.2$ channels (green) with gp130 receptor (red) in DRG neurons in Sham-operation and SNL rats. Arrowheads point to co-labelled neurons. Scale bar = 50 μm. (For interpretation of the references to colour in this figure legend, the reader is referred to the web version of this article.)

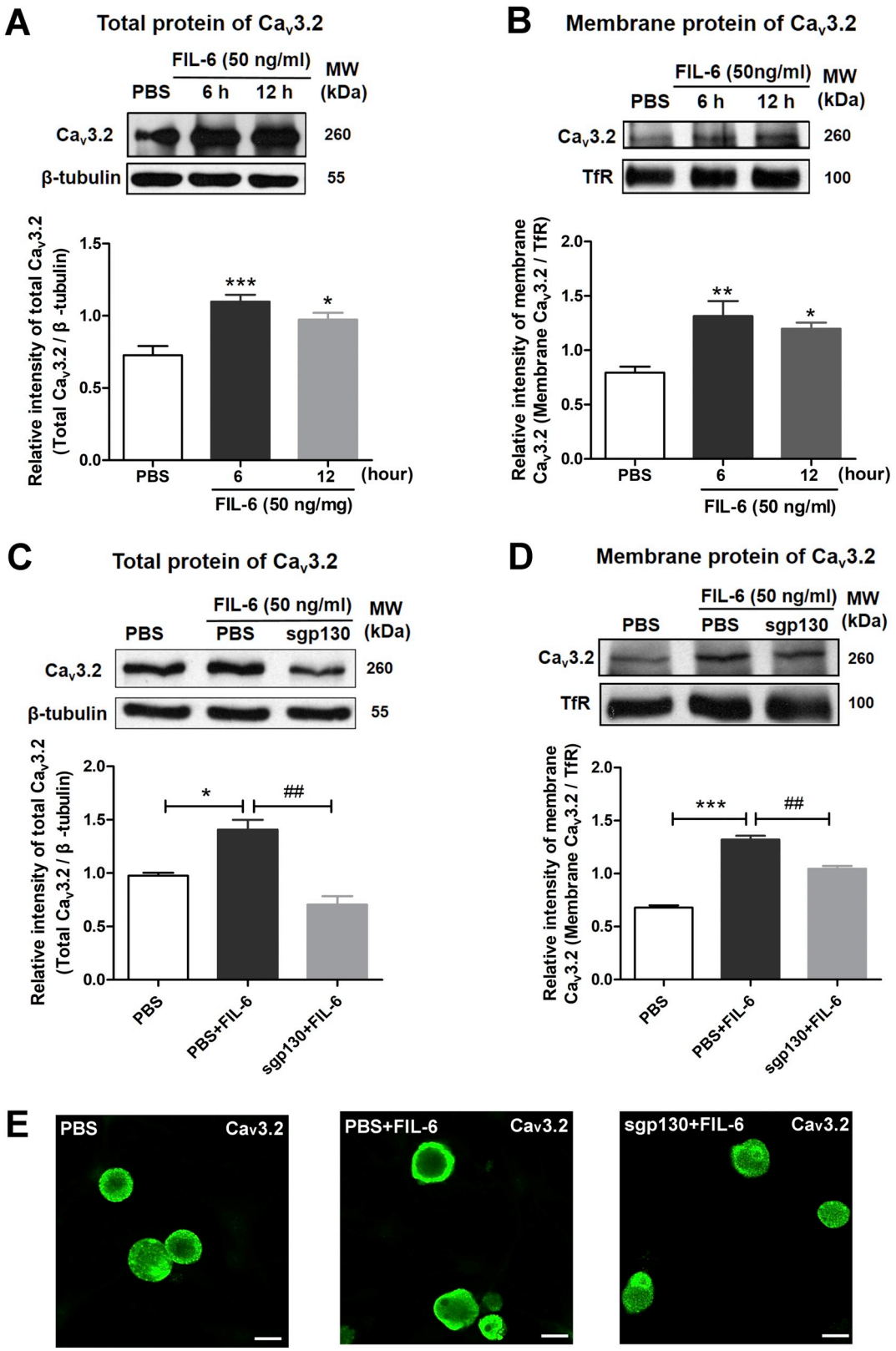

Fig. 7. FIL-6 upregulated expression of $Ca_v3.2$ protein in primary cultured DRG neurons.
(A) Total $Ca_v3.2$ protein. Upper: representative Western blot bands; lower: statistical analysis of total protein expression. FIL-6 incubation for 6–12 h on cultured DRG neurons produced a significant increase compared with the PBS control. n = 7. *p < 0.05, ***p < 0.001, one-way ANOVA with Bonferroni's *post hoc* test. (B) $Ca_v3.2$ membrane protein. Upper: representative Western blot bands; lower: statistical analysis of membrane protein expression. FIL-6 incubation on cultured DRG neurons produced a significant increase of membrane $Ca_v3.2$ compared with the PBS control. n = 6. **p < 0.01, one-way ANOVA with Bonferroni's *post hoc* test. (C, D) FIL-6 incubation for 6 h on primary cultured DRG neurons significantly increased the total and membrane expression of $Ca_v3.2$ protein, but pre-treatment with sgp130, an IL-6/sIL-6 trans-signaling inhibitor, significantly reversed the FIL-6-induced increase of total and membrane $Ca_v3.2$ protein expression. n = 3. *p < 0.05, ***p < 0.001, PBS + FIL-6 vs. PBS control; ##p < 0.01, sgp130 + FIL-6 *vs.* PBS + FIL-6 control, unpaired *t*-test. (E) Representative immunofluorescence images showing FIL-6 incubation for 6 h increased the membrane $Ca_v3.2$ in DRG cells, and sgp130 reversed the increased expression. Scale bar = 20 μm.

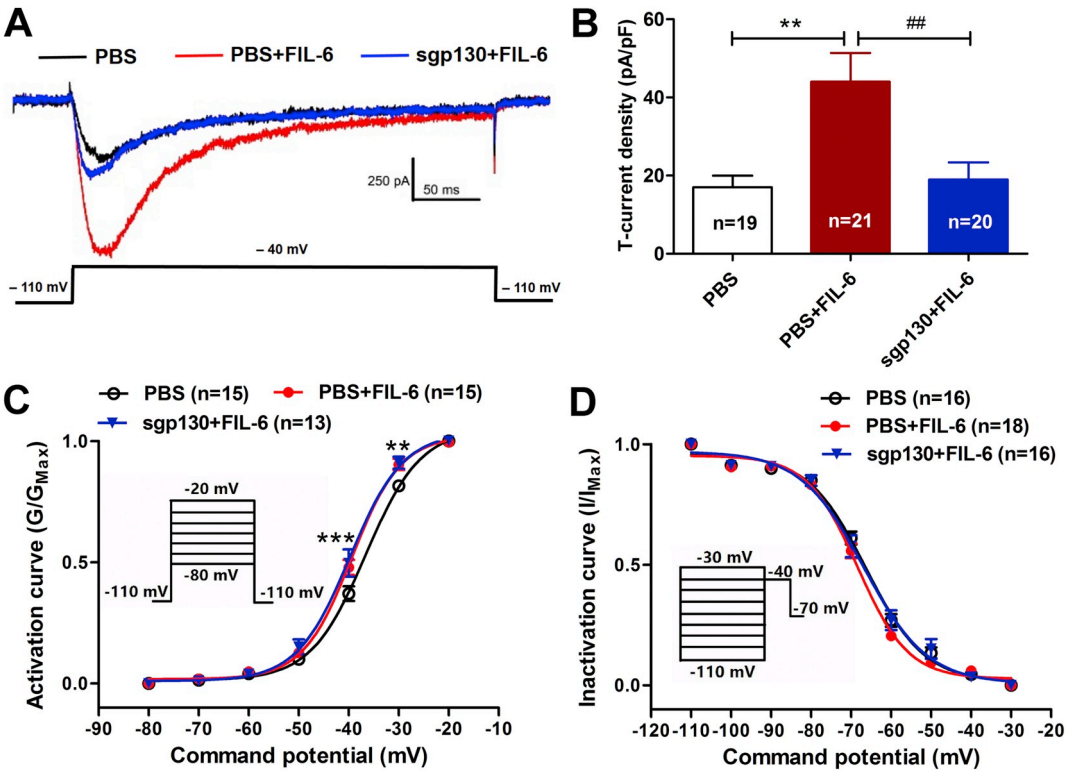

Fig. 8. FIL-6 upregulated function of T-type calcium channels in primary cultured DRG neurons.
(A) Representative traces of T-type calcium currents. (B) FIL-6 evoked a significant increase in T-type Ca^{2+} current densities compared with PBS control, and this FIL-6-induced potentiation of Ca^{2+} currents was markedly blocked by sgp130. n = 19–21. **p < 0.01, PBS + FIL-6 *vs.* PBS; $^{\#\#}$p < 0.01, sgp130 + FIL-6 *vs.* PBS + FIL-6, unpaired *t*-test. (C) FIL-6 elicited an obvious left-shifting of steady-state activation curve, and sgp130 showed no obvious reversal of the left-shifting. n = 13–15. **p < 0.01, ***p < 0.001, PBS + FIL-6 *vs.* PBS, two-way ANOVA with Bonferroni's *post hoc* test. (D) FIL-6 showed no obvious effect on the inactivation curve. Note that the curves in the treatments with PBS, PBS + FIL-6 and sgp130 + FIL-6 overlap almost completely. n = 16–18, two-way ANOVA with Bonferroni's *post hoc* test.

4. Discussion

4.1. $Ca_v3.2$ T-type calcium channels contribute to SNL-induced neuropathic pain

Using *in situ* hybridization (Talley et al., 1999), gene knock-down (Bourinet et al., 2005) and genetic tracing (Bernal Sierra et al., 2017) methods, previous studies have demonstrated that the $Ca_v3.2$ is the predominant subtype of T-type channels in DRG neurons. In the present study, our results showed that $Ca_v3.2$ protein expressed in all three types of DRG neurons in Sham-operation and SNL rats (Fig. 1), suggesting that $Ca_v3.2$ T-type calcium channels are not restricted in the small and medium-sized DRG neurons (Talley et al., 1999). In fact, recent researches reported that $Ca_v3.2$ expressed not only in small and the medium-sized DRG neurons, but also in the large ones. With double immunofluorescent staining, it was shown that 28% $NF200^+$ neurons expressed $Ca_v3.2$ (François et al., 2015). Using $Ca_v3.2$-Cre mice containing fluorescent reporter (tdTomato), it was found that the vast majority (77 ± 4.3%) of $tdTomato^+$ cells expressed NF200 (Bernal Sierra et al., 2017). In addition, Yue et al. found that T-type Ca^{2+} current density significantly increased in medium-sized and large DRG neurons after spared nerve injury (SNI), supporting that $Ca_v3.2$ T-type calcium channels were expressed in all three types of DRG neurons (Yue et al., 2013).

During processing of the nociceptive information, small-diameter DRG neurons are crucial in physiological and pathological pain conditions (Campbell and Meyer, 2006). Large DRG neurons and its fibers usually process touch information in physiological conditions and are also important in tactile allodynia in neuropathic pain after peripheral nerve injury (Xu et al., 2015). More interestingly, in the present study, we found that the percentage of membrane expressing $Ca_v3.2$ increased in all three types of damaged L5 DRG neurons (Fig. 1C–F), suggesting the increased $Ca_v3.2$ channels in all DRG neurons have functional significance.

Our previous study reported that functional up-regulation of $Ca_v3.2$ T-type calcium channels in damaged DRG neurons contributed to neuropathic pain after peripheral nerve injury (Kang et al., 2018). In the present study, we further confirmed the role of these $Ca_v3.2$ T-type calcium channels in neuropathic pain. Our electrophysiological and behavior experiments showed that T-type channel blocker (mibefradil) decreased the ectopic discharge and alleviated mechanical allodynia in a time-dependent manner in SNL rats (Figs. 3 and 5). To double check the effects of T-type calcium channel blocker mibefradil (Bourinet et al., 2016), we further examined the effects of TTA-P2, another novel and selective T-type calcium channel blocker. Consistent with mibefradil, TTA-P2 also reduced ectopic discharges (Fig. 4A–D). Because the vehicle (1.7% DMSO) had obvious behavioral side effects, we did not injected TTA-P2 intrathecally to examine the effects of TTA-P2 (5 mM) on mechanical allodynia. Considering the specificity of mibefradil and TTA-P2 on $Ca_v3.2$ channels, further studies using subtype specific blockers or knockout mice will provide more evidence to this issue. Other subtypes of calcium channels, like $Ca_v3.1$ and $Ca_v3.3$ which are not excluded in the present study, need further investigation.

Emerging evidence demonstrated in addition to the damaged neurons, the adjacent uninjured L4 DRG neurons also contributed to the neuropathic pain (Ma et al., 2003). In our previous studies, we found that $Ca_v3.2$ T-type calcium channels increased in adjacent L4 uninjured DRG neurons in L5 SNL rats (Liu et al., 2018). $Ca_v3.2$ channel proteins are also accumulated in the uninjured sural nerve after SNI and contribute to peripheral sensitization and mechanical allodynia in neuropathic pain (Chen et al., 2018). So, the $Ca_v3.2$ channel is a possible therapeutic target for neuropathic pain.

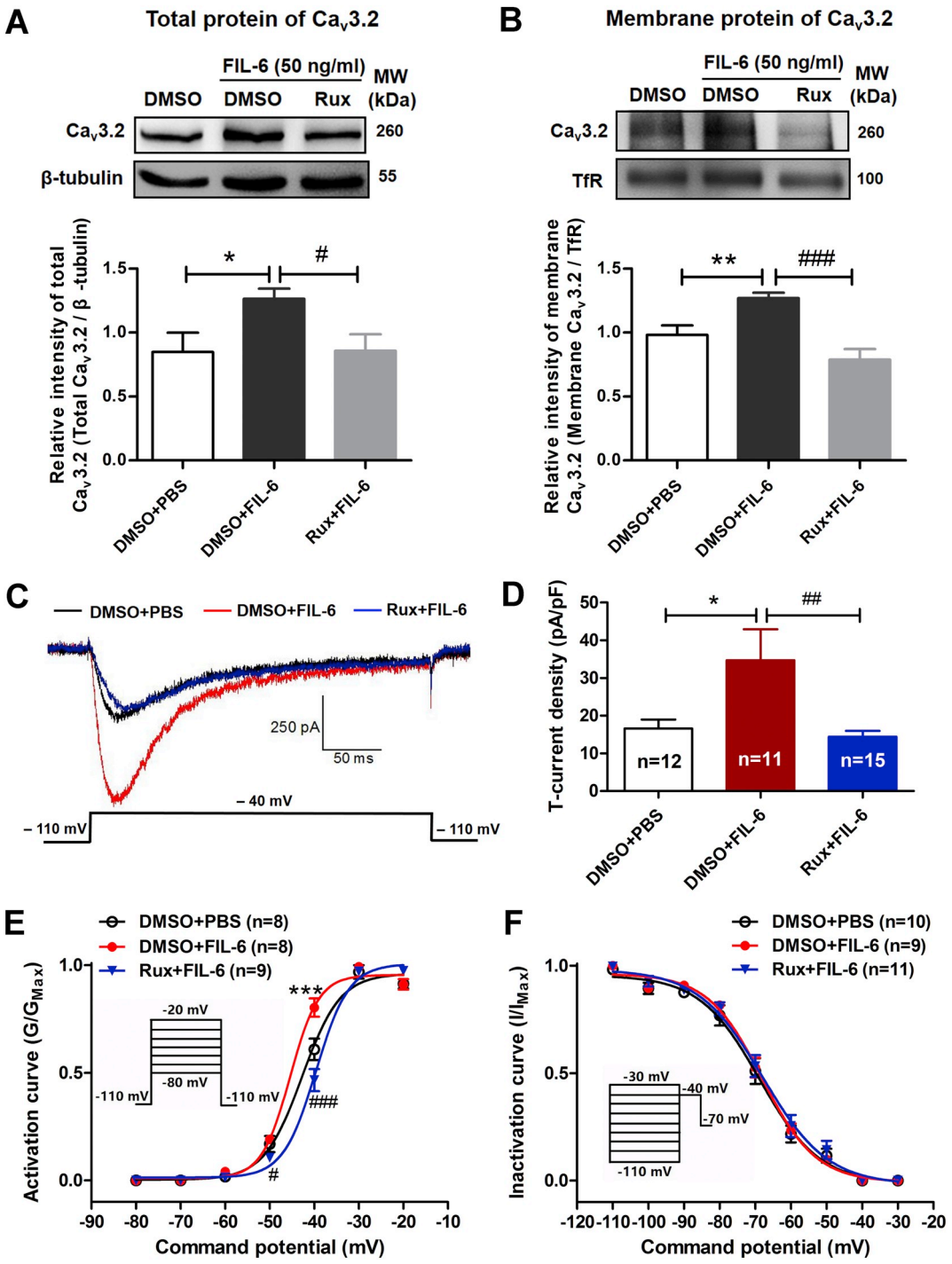

Fig. 9. Ruxolitinib (Rux, a JAK inhibitor) blockade on the FIL-6-evoked upregulation of $Ca_v3.2$ protein expression and function in primary cultured DRG neurons. (A) Total protein expression of $Ca_v3.2$. (B) Membrane protein expression of $Ca_v3.2$. Upper: representative Western blot bands; lower: statistical analysis of $Ca_v3.2$ protein expression. FIL-6 produced a significant increase of total and membrane $Ca_v3.2$, and pre-treatment with ruxolitinib, an IL-6 downstream signal pathway inhibitor, significantly reversed the FIL-6-induced upregulation of total and membrane $Ca_v3.2$ protein. n = 6. *p < 0.05, **p < 0.01, DMSO + FIL-6 vs. DMSO + PBS group; $^{\#}$p < 0.05, $^{\#\#\#}$p < 0.001, Rux + FIL-6 *vs.* DMSO + FIL-6, unpaired *t*-test. (C) Representative traces of T-type calcium currents in primary cultured DRG neurons. (D) Ruxolitinib significantly blocked the FIL-6-induced increase of T-type Ca^{2+} current densities. n = 11–15. *p < 0.05, DMSO + FIL-6 vs. DMSO + PBS; $^{\#\#}$p < 0.01, Rux + FIL-6 *vs.* DMSO + FIL-6, unpaired *t*-test. (E) FIL-6 induced significant left-shifting of the steady-state activation curve, and ruxolitinib reversed this FIL-6 effect. n = 8–9. ***p < 0.01, DMSO + FIL-6 vs. DMSO + PBS; $^{\#}$p < 0.05, $^{\#\#\#}$p < 0.001, Rux + FIL-6 *vs.* DMSO + FIL-6, unpaired *t*-test. (F) No obvious changes were observed in the inactivation curves on DRG neurons treated with DMSO + PBS, DMSO + FIL-6 or Rux + FIL-6. n = 9–11, unpaired *t*-test.

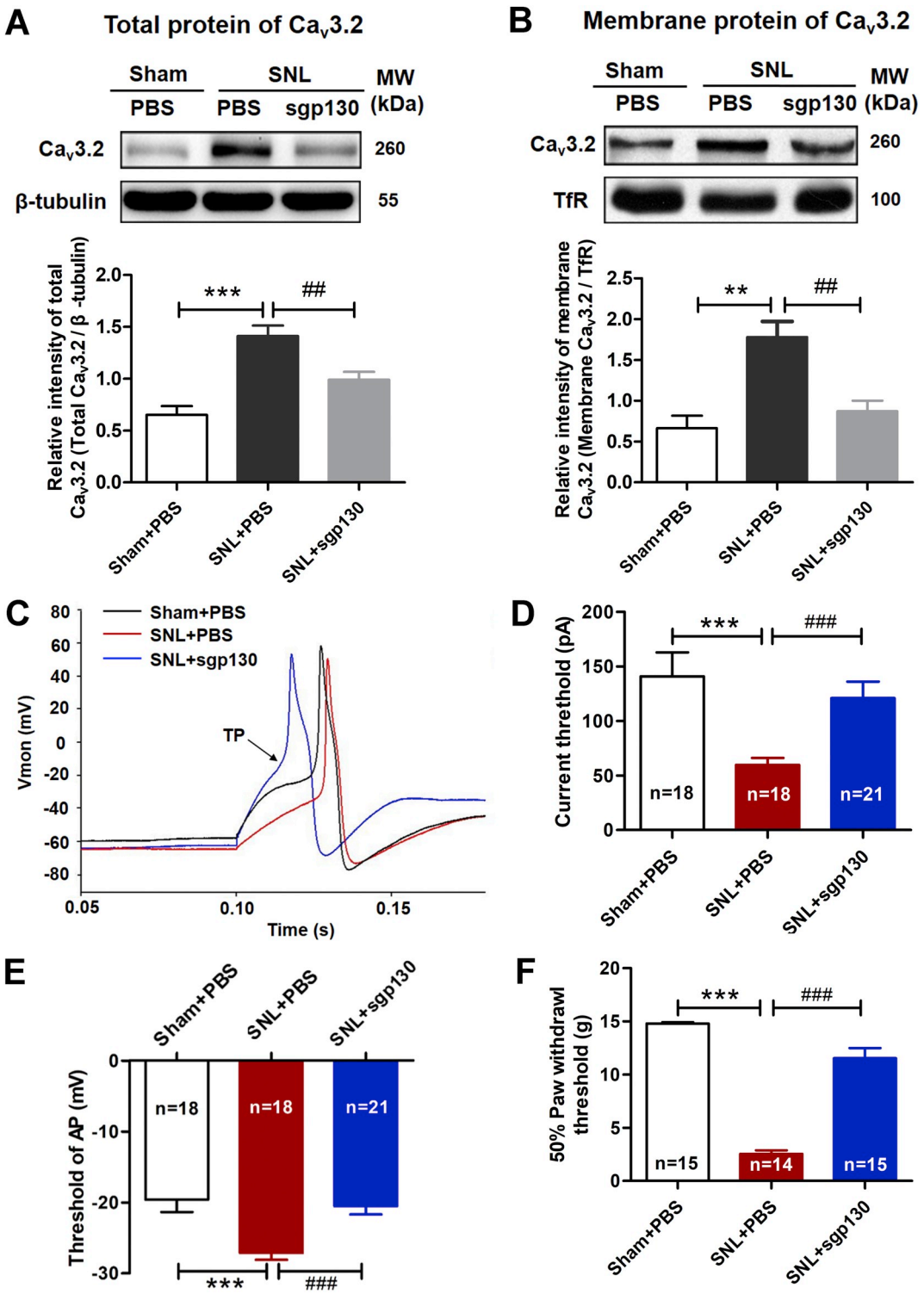

Fig. 10. Sgp130 (an IL-6/sIL-6R signaling inhibitor) reversed the upregulation of $Ca_v3.2$ protein expression in DRG neurons, decreased the hyperexcitability of DRG neurons, and alleviated mechanical allodynia in SNL rats.

(A) Total $Ca_v3.2$ protein expression. (B) Membrane $Ca_v3.2$ protein expression. Upper: representative Western blot bands; lower: statistical analysis of $Ca_v3.2$ protein expression. Sgp130 significantly reversed the upregulation of total and membrane $Ca_v3.2$ protein in DRG neurons compared to the PBS treatment. n = 5–6, $^{**}p < 0.01$, $^{***}p < 0.001$, SNL + PBS *vs.* Sham + PBS; $^{\#\#}p < 0.01$, SNL + sgp130 *vs.* SNL + PBS, unpaired *t*-test. (C-E) Sgp130 decreased the hyperexcitabilities of DRG neurons of SNL rats. Representative traces (C) of the first AP evoked by a series of step depolarizing currents. The depolarizing current threshold for evoking the first AP decreased, and sgp130 reversed this decreased threshold (D). The threshold of AP was also decreased, and reversed by sgp130 (E) in DRG neurons in SNL rats compared with Sham-operation rats. *n* = 18–21, $^{***}p < 0.001$, SNL + PBS *vs.* Sham + PBS; $^{\#\#\#}p < 0.001$, SNL + sgp130 *vs.* SNL + PBS, unpaired *t*-test. (F) Sgp130 alleviated mechanical allodynia in SNL rats. n = 14–15, $^{***}p < 0.001$, SNL + PBS *vs.* Sham + PBS; $^{\#\#\#}p < 0.001$, SNL + sgp130 *vs.* SNL + PBS, unpaired *t*-test.

Taken together, our results further suggest that the increased $Ca_v3.2$ T-type calcium channels in the damaged DRG neurons play important roles in the ectopic discharge, and contribute to neuropathic pain in L5 SNL rats.

4.2. IL-6 through IL-6/sIL-6R signaling pathway upregulates $Ca_v3.2$ T-type calcium channel expression in DRG neurons in neuropathic pain rats after SNL

In order to investigate the underlying mechanisms of $Ca_v3.2$, we investigate whether and how IL-6 regulate the expression and function of $Ca_v3.2$ T-type calcium channels in DRG neurons in neuropathic pain rats after SNL. This is the important goal of our study.

In the nervous system, all microglia and neurons express IL-6 (Lee et al., 2002; März et al., 1998). After injury of peripheral nerves like L5 SNL in our present study, Wallerian degeneration occurred (Wu et al., 2002). Inflammatory mediators (such as IL-1α, IL-1β, IL-6 and tumor necrosis factor-α) were released from activated macrophages, schwann cells, satellite glial cells and axotomized sensory neurons (Kwon et al., 2013; Murphy et al., 1995; Wu et al., 2002). In our experiment, after L5 SNL, IL-6 expression increased significantly from day 1 to day 21 (Fig. 6A). Double immunofluorescence staining was used to examine the IL-6 sources in the DRG, and revealed that both neurons and satellite glial cells contained IL-6 (Fig. 6B). These form the basis of the IL-6 regulation on the $Ca_v3.2$ calcium channels in DRG neurons in neuropathic pain.

In L5 DRG neurons in neuropathic pain rats, $Ca_v3.2$ expression increased, IL-6 expression increased also. Our evidence demonstrated that these two proteins co-localized in the same DRG neurons. For example, $Ca_v3.2$ expressed in all types of DRG neurons (Fig. 1E) and IL-6 co-labelled with the neuronal marker NeuN (Fig. 6B). This kind of co-existence of IL-6 and $Ca_v3.2$ protein in one neuron suggest the possibility that IL-6 could regulate the $Ca_v3.2$ expression. Direct evidence comes from the *in vitro* experiment. In the primary cultured DRG neurons, FIL-6 (a mixture of IL-6 with sIL-6R) induced a significant increase in the total expression and membrane expression of $Ca_v3.2$ from 6 to 12 h after FIL-6 incubation (Fig. 7). These results give strong evidence that IL-6 upregulates $Ca_v3.2$ expression in DRG neurons in neuropathic pain rats.

IL-6 receptors include its specific receptor IL-6R and common receptor gp130. The IL-6R has two isoforms. In addition to the naturally occurring membrane-bound IL-6R (mIL-6R), soluble IL-6R (sIL-6R) has been found (Müllberg et al., 1993, 1994). In some cells on which surface mIL-6R lacks, IL-6 binds to sIL-6R and then activate target cells through the intracellular gp130 (März et al., 1998). gp130 is present essentially in all cell types, mIL-6 receptors are not expressed ubiquitously. So, sIL-6R enriches the cell types that can response to IL-6 by its presence in serum and a number of inflammatory fluids (Rose-John and Heinrich, 1994).

It has been reported that sIL-6R but not mIL-6R was detected in rat DRG (Fang et al., 2015). Thus, we mainly pay attention to the role of IL-6 trans-signaling in regulating $Ca_v3.2$ in this study. We found that FIL-6 (a complex of IL-6 and IL-6R) incubation in the primary cultured DRG neurons significantly increased total and membrane $Ca_v3.2$ protein expression, pretreatment with ruxolitinib (an IL-6 downstream signal pathway inhibitor) could reverse the FIL-6-induced upregulation of $Ca_v3.2$ protein. Furthermore, ruxolitinib markedly blocked the FIL-6-induced increase of Ca^{2+} current densities and reversed the FIL-6 induced left-shifting of the Ca^{2+} current activation curve (Fig. 9). Intrathecal injection of sgp130 reversed the upregulation of total and membrane $Ca_v3.2$ in L5 DRG in neuropathic pain rats induced by SNL (Fig. 10). These results indicate that IL-6 takes its effects through IL-6/sIL-6R/gp130 trans-signaling pathway in the regulation of $Ca_v3.2$ protein expression and trafficking in DRG neurons.

In the present study, intrathecal injection of IL-6 inhibitor (sgp130) attenuated SNL-induced mechanical allodynia. In addition to the peripheral nervous system, IL-6 also regulated central sensitization in the spinal cord. It has been found that spinal administration of IL-6 induced central sensitization and heat hyperalgesia in rats, which was suggested to occur through regulating synaptic and neuronal activity in the superficial spinal cord (Kawasaki et al., 2008). Peripheral nerve injury induced the upregulation of IL-6 in the spinal cord. IL-6 induced spinal glial activation in neuropathic pain (Lee et al., 2010). So, we cannot exclude the effects of intrathecal sgp130 application on spinal cord in our current study. Since our study proved that intrathecal spg130 decreased $Ca_v3.2$ channel expression and neurons hyperexcitability in DRG, these results suggested that the anti-allodynia effect of intrathecal spg130 was mediated very likely through peripheral $Ca_v3.2$ channels.

In addition, in the present study, both sgp130 (an IL-6/sIL-6R signaling inhibitor) and ruxolitinib (an IL-6 downstream signal pathway inhibitor) could reverse the FIL-6-induced upregulation on $Ca_v3.2$ expression (Fig. 7C–E, Fig. 9A and B) and T-type calcium current density (Fig. 8A and B, Fig. 9C and D). It is also noticed that sgp130 could not reverse the FIL-6-induced left-shifting of activation curve (Fig. 8C), but ruxolitinib could (Fig. 9E). This discrepancy can not be fully explained from the present results or literatures. Whether or not there are other signals participating into this regulation need further investigation.

A previous study reported that IL-6 synthesis increased the sensitivity of sensory neurons to axotomy (Murphy et al., 1995; Ramer et al., 1998). In bone cancer pain model of rats, IL-6 upregulated TRPV1 expression and the hyperexcitability of DRG neurons (Fang et al., 2015). In our study, *in vivo* extracellular electrophysiological recordings on teased fibers showed that blockade of T-type calcium channels with antagonist mibefradil (Fig. 3) or TTA-P2 (Fig. 4) inhibited the ectopic discharges in the nerve fibers in SNL rats. FIL-6 evoked a significant increase in T-type Ca^{2+} current densities, and this FIL-6-induced potentiation of Ca^{2+} currents was markedly blocked by sgp130 (Fig. 8). Thresholds for the AP induction were significantly decreased in DRG neurons in SNL rats, and sgp130 almost completely blocked this phenomenon (Fig. 10). These results suggest that IL-6 upregulates the $Ca_v3.2$-mediated neuronal excitability in neuropathic pain rats after SNL.

Our present results demonstrate that IL-6-upregulated $Ca_v3.2$ contributes to neuropathic pain. In IL-6 knockout mice, sympathetic sprouting induced by nerve injury was significantly reduced, and thus mechanical allodynia was markedly delayed, implying a facilitatory role for IL-6 in pain (Murphy et al., 1995; Ramer et al., 1998). It has been reported that IL-6 antibody combined with corticotropin-releasing factor receptor 1 receptor antagonist reduced $Ca_v3.2$ channel expression and normalized visceral pain in rat model of irritable bowel syndrome (Buckley et al., 2014). In our present study, intrathecal application of sgp130, an inhibitor of IL-6/IL-6R/gp130 signaling pathway, could reverse the upregulation of membrane $Ca_v3.2$ expression (Fig. 7), the hyperexcitability of DRG neurons as well as mechanical allodynia in SNL neuropathic pain rats (Fig. 10).

5. Conclusions

Our present study suggest that IL-6 upregulates $Ca_v3.2$ T-type channels expression and function through the IL-6/IL-6R/gp130 trans-signaling pathway in DRG neurons, thus contributes to the development of neuropathic pain in rats after peripheral nerve injury (Fig. 11).

Supplementary data to this article can be found online at https://doi.org/10.1016/j.expneurol.2019.03.005.

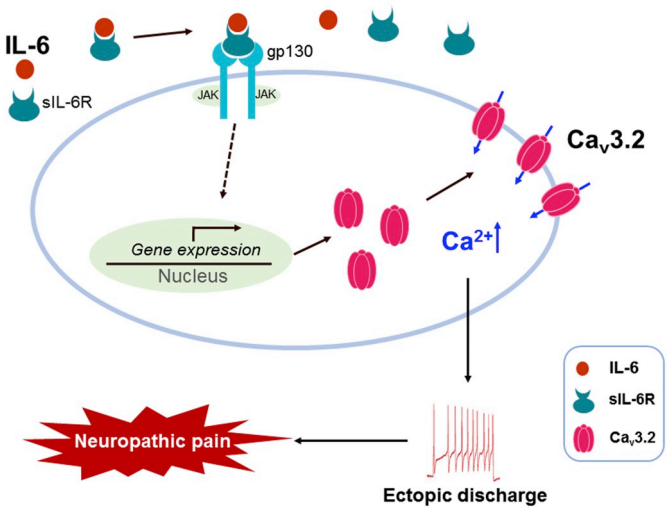

Fig. 11. A schematic of interleukin-6 (IL-6)-mediated upregulation of $Ca_v3.2$ T-type channels through IL-6/sIL-6R trans-signaling in dorsal root ganglion (DRG) neurons in the development of neuropathic pain.
The expression of IL-6 and gp130 increases significantly in DRG after spinal nerve ligation (SNL). The elevated IL-6 binds to sIL-6R and induces homodimerization of gp130, which subsequently activates the JAK signaling cascade and then triggers the functional upregulation of $Ca_v3.2$ T-type channels. The potentiated $Ca_v3.2$ T-type channels lead to an increase in calcium influx, and then result in ectopic discharges of DRG neurons and pain behaviors of neuropathic pain rats.

Acknowledgments

This work was supported by grants from National Key R&D Program of China (2017YFA0701302), National Natural Science Foundation of China (31371119, 91732107, 81571067 and 81521063), National Basic Research Program of China (2015CB554503), "111" Project of Ministry of Education of China (B07001), and the Interdisciplinary Medicine Seed Fund of Peking University (BMU2018MX011).

Conflict of interests

Authors declare no conflicts of interests.

Authors' contribution.

QYL, WC, FYL and YW designed the experiment; WC, QYL, XCF, JXW, SF, SC, FFL, JC, XHW, YHH, LS, LJZ, FYL performed the experiments; WC, QYL, LJZ, LS, FYL and MY analyzed the data; QYL, WC, FYL and YW wrote the manuscript.

References

Becker, A.J., Pitsch, J., Sochivko, D., Opitz, T., Staniek, M., Chen, C.C., Campbell, K.P., Schoch, S., Yaari, Y., Beck, H., 2008. Transcriptional upregulation of $Ca_v3.2$ mediates epileptogenesis in the pilocarpine model of epilepsy. J. Neurosci. 28, 13341–13353.
Bernal Sierra, Y.A., Haseleu, J., Kozlenkov, A., Bégay, V., Lewin, G.R., 2017. Genetic tracing of $Ca_v3.2$ T-type calcium channel expression in the peripheral nervous system. Front. Mol. Neurosci. 10, 70.
Bourinet, E., Alloui, A., Monteil, A., Barrère, C., Couette, B., Poirot, O., Pages, A., McRory, J., Snutch, T.P., Eschalier, A., Nargeot, J., 2005. Silencing of the $Ca_v3.2$ T-type calcium channel gene in sensory neurons demonstrates its major role in nociception. EMBO J. 24, 315–324.
Bourinet, E., Francois, A., Laffray, S., 2016. T-type calcium channels in neuropathic pain. Pain 157, S15–S22.
Buckley, M.M., O'Halloran, K.D., Rae, M.G., Dinan, T.G., O'Malley, D., 2014. Modulation of enteric neurons by interleukin-6 and corticotropin-releasing factor contributes to visceral hypersensitivity and altered colonic motility in a rat model of irritable bowel syndrome. J. Physiol. 592, 5235–5250.
Campbell, J.N., Meyer, R.A., 2006. Mechanisms of neuropathic pain. Neuron 52, 77–92.
Catterall, W.A., 2010. Ion channel voltage sensors: structure, function, and pathophysiology. Neuron 67, 915–928.
Chaplan, S.R., Bach, F.W., Pogrel, J.W., Chung, J.M., Yaksh, T.L., 1994. Quantitative assessment of tactile allodynia in the rat paw. J. Neurosci. Methods 53, 55–63.
Chen, W., Chi, Y.N., Kang, X.J., Liu, Q.Y., Zhang, H.L., Li, Z.H., Zhao, Z.F., Yang, Y., Su, L., Cai, J., Liao, F.F., Yi, M., Wan, Y., Liu, F.Y., 2018. Accumulation of $Ca_v3.2$ T-type calcium channels in the uninjured sural nerve contributes to neuropathic pain in rats with spared nerve injury. Front. Mol. Neurosci. 11, 24.
Dixon, W.J., 1980. Efficient analysis of experimental observations. Annu. Rev. Pharmacol. Toxicol. 20, 441–462.
Fang, D., Kong, L.Y., Cai, J., Li, S., Liu, X.D., Han, J.S., Xing, G.G., 2015. Interleukin-6-mediated functional upregulation of TRPV1 receptors in dorsal root ganglion neurons through the activation of JAK/PI3K signaling pathway: roles in the development of bone cancer pain in a rat model. Pain 156, 1124–1144.
François, A., Schüetter, N., Laffray, S., Sanguesa, J., Pizzoccaro, A., Dubel, S., Mantilleri, A., Nargeot, J., Noël, J., Wood, J.N., Moqrich, A., Pongs, O., Bourinet, E., 2015. The low-threshold calcium channel $Ca_v3.2$ determines low-threshold mechanoreceptor function. Cell Rep. 10, 370–382.
Heinrich, P.C., Behrmann, I., Haan, S., Hermanns, H.M., Müller-Newen, G., Schaper, F., 2003. Principles of interleukin (IL)-6-type cytokine signalling and its regulation. Biochem. J. 374, 1–20.
Hirano, T., Taga, T., Nakano, N., Yasukawa, K., Kashiwamura, S., Shimizu, K., Nakajima, K., Pyun, K.H., Kishimoto, T., 1985. Purification to homogeneity and characterization of human B-cell differentiation factor (BCDF or BSFp-2). Proc. Natl. Acad. Sci. U. S. A. 82, 5490–5494.
Jagodic, M.M., Pathirathna, S., Nelson, M.T., Mancuso, S., Joksovic, P.M., Rosenberg, E.R., Bayliss, D.A., Jevtovic-Todorovic, V., Todorovic, S.M., 2007. Cell-specific alterations of T-type calcium current in painful diabetic neuropathy enhance excitability of sensory neurons. J. Neurosci. 27, 3305–3316.
Jagodic, M.M., Pathirathna, S., Joksovic, P.M., Lee, W., Nelson, M.T., Naik, A.K., Su, P., Jevtovic-Todorovic, V., Todorovic, S.M., 2008. Upregulation of the T-type calcium current in small rat sensory neurons after chronic constrictive injury of the sciatic nerve. J. Neurophysiol. 99, 3151–3156.
Jiang, Y.Q., Xing, G.G., Wang, S.L., Tu, H.Y., Chi, Y.N., Li, J., Liu, F.Y., Han, J.S., Wan, Y., 2008. Axonal accumulation of hyperpolarization-activated cyclic nucleotide-gated cation channels contributes to mechanical allodynia after peripheral nerve injury in rat. Pain 137, 495–506.
Joksimovic, S.L., Joksimovic, S.M., Tesic, V., Garcia-Caballero, A., Feseha, S., Zamponi, G.W., Jevtovic-Todorovic, V., Todorovic, S.M., 2018. Selective inhibition of $Ca_v3.2$ channels reverses hyperexcitability of peripheral nociceptors and alleviates postsurgical pain. Sci. Signal. 11 (pii: eaao4425).
Kang, X.J., Chi, Y.N., Chen, W., Liu, F.Y., Cui, S., Liao, F.F., Cai, J., Wan, Y., 2018. Increased expression of $Ca_v3.2$ T-type calcium channels in damaged DRG neurons contributes to neuropathic pain in rats with spared nerve injury. Mol. Pain 14, 1–11.
Kawasaki, Y., Zhang, L., Cheng, J.K., Ji, R.R., 2008. Cytokine mechanisms of central sensitization: distinct and overlapping role of interleukin-1beta, interleukin-6, and tumor necrosis factor-alpha in regulating synaptic and neuronal activity in the superficial spinal cord. J. Neurosci. 28, 5189–5194.
Kim, S.H., Chung, J.M., 1992. An experimental model for peripheral neuropathy produced by segmental spinal nerve ligation in the rat. Pain 50, 355–363.
Kwon, M.J., Kim, J., Shin, H., Jeong, S.R., Kang, Y.M., Choi, J.Y., Hwang, D.H., Kim, B.G., 2013. Contribution of macrophages to enhanced regenerative capacity of dorsal root ganglia sensory neurons by conditioning injury. J. Neurosci. 33, 15095–15108.
Latrémolière, A., Mauborgne, A., Masson, J., Bourgoin, S., Kayser, V., Hamon, M., Pohl, M., 2008. Differential implication of proinflammatory cytokine interleukin-6 in the development of cephalic versus extracephalic neuropathic pain in rats. J. Neurosci. 28, 8489–8501.
Lee, Y.B., Nagai, A., Kim, S.U., 2002. Cytokines, chemokines, and cytokine receptors in human microglia. J. Neurosci. Res. 69, 94–103.
Lee, K.M., Jeon, S.M., Cho, H.J., 2010. Interleukin-6 induces microglial CX3CR1 expression in the spinal cord after peripheral nerve injury through the activation of p38 MAPK. Eur. J. Pain 14, 682.
Li, Y., Tatsui, C.E., Rhines, L.D., North, R.Y., Harrison, D.S., Cassidy, R.M., Johansson, C.A., Kosturakis, A.K., Edwards, D.D., Zhang, H., Dougherty, P.M., 2017. Dorsal root ganglion neurons become hyperexcitable and increase expression of voltage-gated T-type calcium channels ($Ca_v3.2$) in paclitaxel-induced peripheral neuropathy. Pain 158, 417–429.
Liu, F.Y., Qu, X.X., Ding, X., Cai, J., Jiang, H., Wan, Y., Han, J.S., Xing, G.G., 2010. Decrease in the descending inhibitory 5-HT system in rats with spinal nerve ligation. Brain Res. 1330, 45–60.
Liu, F.Y., Qu, X.X., Cai, J., Wang, F.T., Xing, G.G., Wan, Y., 2011. Electrophysiological properties of spinal wide dynamic range neurons in neuropathic pain rats following spinal nerve ligation. Neurosci. Bull. 27, 1–8.
Liu, F.Y., Sun, Y.N., Wang, F.T., Li, Q., Su, L., Zhao, Z.F., Meng, X.L., Zhao, H., Wu, X., Sun, Q., Xing, G.G., Wan, Y., 2012. Activation of satellite glial cells in lumbar dorsal root ganglia contributes to neuropathic pain after spinal nerve ligation. Brain Res. 1427, 65–77.
Liu, Q.Y., Chen, W., Cui, S., Liao, F.F., Yi, M., Liu, F.Y., Wan, Y., 2018. Upregulation of $Ca_v3.2$ T-type calcium channels in adjacent intact L4 dorsal root ganglion neurons in neuropathic pain rats with L5 spinal nerve ligation. Neurosci. Res. https://doi.org/10.1016/j.neures.2018.04.002.
Ma, C., Shu, Y.Z., Chen, Y., Yao, H., Greenquist, K.W., White, F.A., LaMotte, R.H., 2003. Similar electrophysiological changes in axotomized and neighboring intact dorsal root ganglion neurons. J. Neurophysiol. 89, 1588–1602.
März, P., Cheng, J.G., Gadient, R.A., Patterson, P.H., Stoyan, T., Otten, U., Rose-John, S., 1998. Sympathetic neurons can produce and respond to interleukin 6. Proc. Natl. Acad. Sci. U. S. A. 95, 3251–3256.
Messinger, R.B., Naik, A.K., Jagodic, M.M., Nelson, M.T., Lee, W.Y., Choe, W.J., Orestes, P., Latham, J.R., Todorovic, S.M., Jevtovic-Todorovic, V., 2009. In vivo silencing of the $Ca_v3.2$ T-type calcium channels in sensory neurons alleviates hyperalgesia in rats

with streptozocin-induced diabetic neuropathy. Pain 145, 184–195.
Müllberg, J., Schooltink, H., Stoyan, T., Gunther, M., Graeve, L., Buse, G., Mackiewicz, A., Heinrich, P.C., Rose-John, S., 1993. The soluble interleukin-6 receptor is generated by shedding. Eur. J. Immunol. 23, 473–480.
Müllberg, J., Oberthür, W., Lottspeich, F., Mehl, E., Dittrich, E., Craeve, L., Heinrich, P.C., Rose-John, S., 1994. The soluble human IL-6 receptor. Mutational characterization of the proteolytic cleavage site. J. Immunol. 152, 4958–4968.
Murphy, P.G., Grondin, J., Altares, M., Richardson, P.M., 1995. Induction of interleukin-6 in axotomized sensory neurons. J. Neurosci. 15, 5130–5138.
Natura, G., von Banchet, G.S., Schaible, H.G., 2005. Calcitonin gene-related peptide enhances TTX-resistant sodium currents in cultured dorsal root ganglion neurons from adult rats. Pain 116, 194–204.
Nelson, M.T., Joksovic, P.M., Su, P., Kang, H.W., Van Deusen, A., Baumgart, J.P., David, L.S., Snutch, T.P., Barrett, P.Q., Lee, J.H., Zorumski, C.F., Perez-Reyes, E., Todorovic, S.M., 2007. Molecular mechanisms of subtype-specific inhibition of neuronal T-type calcium channels by ascorbate. J. Neurosci. 27, 12577–12583.
Obradovic, A.L., Hwang, S.M., Scarpa, J., Hong, S.J., Todorovic, S.M., Jevtovic-Todorovic, V., 2014. $Ca_v3.2$ T-type calcium channels in peripheral sensory neurons are important for mibefradil-induced reversal of hyperalgesia and allodynia in rats with painful diabetic neuropathy. PLoS One 9, e91467.
Ramer, M.S., Murphy, P.G., Richardson, P.M., Bisby, M.A., 1998. Spinal nerve lesion-induced mechanoallodynia and adrenergic sprouting in sensory ganglia are attenuated in interleukin-6 knockout mice. Pain. 78, 115–121.
Rose-John, S., 2012. IL-6 trans-signaling via the soluble IL-6 receptor: importance for the pro-inflammatory activities of IL-6. Int. J. Biol. Sci. 8, 1237–1247.
Rose-John, S., Heinrich, P.C., 1994. Soluble receptors for cytokines and growth factors: generation and biological function. Biochem. J. 300, 281–290.
Rose-John, S., Scheller, J., Elson, G., Jones, S.A., 2006. Interleukin-6 biology is coordinated by membrane-bound and soluble receptors: role in inflammation and cancer. J. Leukoc. Biol. 80, 227–236.
Rothaug, M., Becker-Pauly, C., Rose-John, S., 2016. The role of interleukin-6 signaling in nervous tissue. Biochim. Biophys. Acta 1863, 1218–1227.
Scheller, J., Rose-John, S., 2006. Interleukin-6 and its receptor: from bench to bedside. Med. Microbiol. Immunol. 195, 173–183.
Sun, Q., Tu, H., Xing, G.G., Han, J.S., Wan, Y., 2005. Ectopic discharges from injured nerve fibers are highly correlated with tactile allodynia only in early, but not late, stage in rats with spinal nerve ligation. Exp. Neurol. 191, 128–136.
Taga, T., Kishimoto, T., 1997. Gp130 and the interleukin-6 family of cytokines. Annu. Rev. Immunol. 15, 797–819.
Takahashi, T., Aoki, Y., Okubo, K., Maeda, Y., Sekiguchi, F., Mitani, K., Nishikawa, H., Kawabata, A., 2010. Upregulation of $Ca_v3.2$ T-type calcium channels targeted by endogenous hydrogen sulfide contributes to maintenance of neuropathic pain. Pain 150, 183–191.
Talley, E.M., Cribbs, L.L., Lee, J.H., Daud, A., Perez-Reyes, E., Bayliss, D.A., 1999. Differential distribution of three members of a gene family encoding low voltage-activated (T-type) calcium channels. J. Neurosci. 19, 1895–1911.
Tian, N.X., Xu, Y., Yang, J.Y., Li, L., Sun, X.H., Wang, Y., Zhang, Y., 2018. KChIP3 N-terminal 31-50 fragment mediates its association with TRPV1 and alleviates inflammatory hyperalgesia in rats. J. Neurosci. 38, 1756–1773.
Tyrrell, L., Renganathan, M., Dib-Hajj, S.D., Waxman, S.G., 2001. Glycosylation alters steady-state inactivation of sodium channel Nav1.9/NaN in dorsal root ganglion neurons and is developmentally regulated. J. Neurosci. 21, 9629–9637.
Weaver, E.M., Zamora, F.J., Hearne, J.L., Martin-Caraballo, M., 2015. Posttranscriptional regulation of T-type Ca^{2+} channel expression by interleukin-6 in prostate cancer cells. Cytokine 76, 309–320.
Wen, X.J., Xu, S.Y., Chen, Z.X., Yang, C.X., Liang, H., Li, H., 2010. The roles of T-type calcium channel in the development of neuropathic pain following chronic compression of rat dorsal root ganglia. Pharmacology 85, 295–300.
Wolf, J., Rose-John, S., Garbers, C., 2014. Interleukin-6 and its receptors: a highly regulated and dynamic system. Cytokine 70, 11–20.
Wu, G., Ringkamp, M., Murinson, B.B., Pogatzki, E.M., Hartke, T.V., Weerahandi, H.M., Campbell, J.N., Griffin, J.W., Meyer, R.A., 2002. Degeneration of myelinated efferent fibers induces spontaneous activity in uninjured C-fiber afferents. J. Neurosci. 22, 7746–7753.
Xiao, X., Zhao, X.T., Xu, L.C., Yue, L.P., Liu, F.Y., Cai, J., Liao, F.F., Kong, J.G., Xing, G.G., Yi, M., Wan, Y., 2015. Shp-1 dephosphorylates TRPV1 in dorsal root ganglion neurons and alleviates CFA-induced inflammatory pain in rats. Pain 156, 597–608.
Xu, Z.Z., Kim, Y.H., Bang, S., Zhang, Y., Berta, T., Wang, F., Oh, S.B., Ji, R.R., 2015. Inhibition of mechanical allodynia in neuropathic pain by TLR5-mediated A-fiber blockade. Nat. Med. 21, 1326–1331.
Yu, L., Yang, F., Luo, H., Liu, F.Y., Han, J.S., Xing, G.G., Wan, Y., 2008. The role of TRPV1 in different subtypes of dorsal root ganglion neurons in rat chronic inflammatory nociception induced by complete Freund's adjuvant. Mol. Pain 4, 61.
Yue, J., Liu, L., Liu, Z., Shu, B., Zhang, Y., 2013. Upregulation of T-type Ca^{2+} channels in primary sensory neurons in spinal nerve injury. Spine 38, 463–470.
Zhang, Y., Qin, W.J., Qian, Z.Y., Liu, X.J., Wang, H., Gong, S., Sun, Y.G., Snutch, T.P., Jiang, X.H., Tao, J., 2014. Peripheral pain is enhanced by insulin-like growth factor 1 through a G protein-mediated stimulation of T-type calcium channels. Sci. Signal. 7, ra94.
Zimmermann, M., 1983. Ethical guidelines for investigations of experimental pain in conscious animals. Pain 16, 109–110.